IMAGING FIBER ORIENTATION IN ARTICULAR CARTILAGE USING OPTICAL POLARIZATION TRACTOGRAPHY

A Thesis presented to

the Faculty of the Graduate School

at the University of Missouri

In Partial Fulfillment of the Requirements for the Degree

Master of Science

---

by

XUAN YAO

Dr. Gang Yao, Thesis Supervisor

MAY 2016

The undersigned, appointed by the dean of the Graduate School, have examined the thesis entitled

IMAGING FIBER ORIENTATION OF ARTICULAR CARTILAGE USING OPTICAL POLARIZATION TRACTOGRAPHY

Presented by Xuan Yao,

a candidate for the degree of Master of Science,

and hereby certify that, in their opinion, it is worthy of acceptance.

Professor Gang Yao, Department of Bioengineering

Professor Ferris M. Pfeiffer, Department of Bioengineering and Department of Orthopaedic Surgery

---

Professor Dongsheng Duan, Department of Molecular Microbiology & Immunology

ACKNOWLEDGEMENTS

First, I would like to express my gratitude to my advisor Dr. Gang Yao who provided me the great opportunity to extend my education and to study in the field of optical imaging. I thank him for all the support, professional guidance, and inspiration for future direction he provided. I have learned a lot from him on how to be an independent researcher, and what is dedication and diligence to the career of research. I also thank Dr. Ferris M. Pfeiffer and Dr. Dongsheng Duan for serving on my committee and for their advice in my research.

I want to express my thanks to my lab colleague Yuanbo Wang, for his stimulating advice and pleasant collaboration in research. Also, I want to thank my current colleagues Leila Azinfar, Mohammadreza Ravanfar, and Randima M. Dinalankara for their valuable help during my studies. I want to give special thanks to the meat lab manager Rick Disselhorst for his help of providing cartilage samples.

Finally, I want to thank my friends and family for their endless support and help during my two years' graduate study abroad. They always stand by my side and give me great happiness and confidence.

TABLE OF CONTENTS

ACKNOWLEDGEMENTS II

LIST OF FIGURES V

LIST OF TABLES VII

ABSTRACT VIII

CHAPTER 1. BACKGROUND AND INTRODUCTION 1

1.1. Articular cartilage 1

1.1.1. Osteoarthritis: diagnosis and treatment 3

1.1.2. Cartilage imaging 4

1.2. The "split-line" map of cartilage 5

1.2.1. Creation of split-lines 5

1.2.2. Interpretation of split-lines 6

1.3. Imaging based on optical coherence tomography (OCT) 8

1.3.1. Polarization Sensitive Optical Coherence Tomography (PS-OCT) 9

1.3.2. Fundamentals of optical polarization 10

1.3.3. Jones Matrix description of polarization light 11

1.3.4. Birefringence 12

1.3.5. OCT and PS-OCT imaging of cartilage 14

1.4. Contribution of this thesis research 15

CHAPTER 2. EXPERIMENTAL METHODS 16

2.1. Optical Polarization Tractography (OPT) 16

2.1.1. Imaging system 16

2.1.2. Optical Axis Calculation 18

2.2. Split-line generation and analysis 20

2.2.1. Needle Choice 20

2.2.2. Split line images and quantification 22

2.2.3. Correlation between split line OPT 24

CHAPTER 3. RESULTS AND DISCUSSIONS 26

3.1. Cartilage samples 26
3.2. Top Scan Intensity image and split line fitting 27
3.3. Fiber orientation from optical polarization tractography (OPT) 28
3.4. Correlation Analysis 29
3.5. Best Correlated Depth 33
3.6. Thickness measurement from Top Scan 34
3.7. Discussions 36
3.7.1. Scan the sample from side 36
3.7.2. Histology Validation 38
3.7.3. Thickness Measurement Summary 39
3.7.4. The goodness of fitting 40
3.8. Summary 42
CHAPTER 4. CONCLUSIONS AND FUTURE STUDIES 46
REFERENCES 47
APPENDIX 51

LIST OF FIGURES

Figure 1-1. Different split line patterns observed in our study. (a)Straight split line; (b) Curved split line; (c) Sharply angled, forked split line; and (d) Stellate split line. .. 6

Figure 1-2. A schematic diagram of the OCT system. In Fourier domain OCT, the A-scan is obtained using direct Fourier transform of the interference signal..... 9

Figure 1-3. Diagrams of (a) linear polarization, (b) circular polarization, and (c) elliptical polarization. This diagram is from Wikipedia, the copyright holder of this file allows anyone to use it for any purpose..... 11

Figure 1-4. Illustration of (a) Isotropic crystal ($n_1=n_2=n_3=n_0$) and (b) Uniaxial crystal where $n_e \neq n_0$. 13

Figure 2-1. A schematic diagram of the PS-OCT system. SLD: Superluminescent diode; C: collimator, P: a polarizer for generating vertically polarized light; EOM: electronic optical modulator; BS: non polarization beam splitter; ND: neutral density filter; PBS: polarization beam splitter; M1, M2: reference mirrors for the horizontal and vertical polarization components; L1: achromatic collimation lens (f = 30 mm); L2 achromatic focusing lens (f = 120 mm); OL: objective lens (f = 60 mm); VPHTG: volume phase holography transmission grating (1200lines/mm)..... 16

Figure 2-2. (a) Split line patterns created by injection needle with two perpendicular directions. (b) Example image of injection needle with tip (red circled area). The orientation of split line changes with the alteration of tip direction (red circled part). (c) Intensity image of split line pattern created by dissecting needle; (d) Example image of dissecting needle. (e) Intensity image of split line pattern created by conical needle with fine tip; (f) Example image of conical needle with fine tip. 21

Figure 2-3. Illustration of procedures of fitting: (a) Choose ROI from *en face* intensity image; (b) Create a binary image of ROI; (c) Get the greyscale image of ROI and extract split line in ROI; (d) Get the split line binary mask; (e) Get the equivalent area from optical axis image, represented with HSV colormap. 23

Figure 3-1. Photo of dissected cartilage sample from the first phalanges in pig foot. 27

Figure 3-2. (a) Articular cartilage from pig first phalanges with split line patterns. Yellow square area (6*6mm) was scanned on sample #0105161; (b) *en face* intensity image of sample; (c) Fitting result plotted over the intensity image with a red dashed line; (d) Fitted split line plot with a white background. 28

Figure 3-3. (a) *en face* axis image from depth of 48μm. Axis was shown in hsv color ranging from -90° to 90°. (b) The streamline plotted overlaid on the intensity

image..... 29

Figure 3-4. Correlation curve of sample 01051601 (OPT vs. Split Line). (a) Correlation curve at 48µm; (b) Correlation curve at 56µm; (c) Correlation curve at 64µm; (d) Correlation curve at 72µm; Correlation analysis result of sample 01051601 (0-600µm). (e) Distribution of R^2; (f) distribution of RMSE..... 31

Figure 3-5. (a) Articular cartilage from pig with split line patterns, yellow square area (6*6mm) of sample #01241602; (b) *en face* intensity image of sample; (c) Fitting result plotted over the intensity image with a red dashed line; (d) Fitted split line plot with a white background..... 32

Figure 3-6. (a) *en face* axis image from another sample #01241602 at depth of 48µm; (b) streamline plotted over intensity image. 33

Figure 3-7. Correlation results from five different cartilage samples at (a) depth 48µm with 0.9506 as value of R^2 and 1.0255 as value of slope; (b) depth 56µm with 0.9539 as value of R^2 and 1.0109 as value of slope; (c) depth 64µm with 0.9462 as value of R^2 and 1.0069 as value of slope; (d) depth 72µm with 0.933 as value of R^2 and 1.0024 as value of slope..... 34

Figure 3-8. Local Retardation averaged from one cross-section from middle of the sample image plotted over the depth in sample #01051601 35

Figure 3-9. (a) Decalcified sample was cut from the sample shown in Figure 3-2; (b) Mark 1 part was the sample #0105161. The images obtained from the yellow squared area are shown with (c) intensity image, (d) optical axis, and (e) streamline plotted on intensity image at transmural depth of 180µm..... 37

Figure 3-10. (a) Cartilage histology image with H&E stain shown in 10x magnification. Yellow line marks the thickness of 560µm, green line marks the thickness of 500µm; (b) Cartilage histology image was shown in 20x magnification. Yellow line marks the superficial layer and thickness here is 115µm; (c) Cartilage histology image was shown in 20x magnification. Green line marks the superficial layer and thickness here is 95µm. 39

Figure 3-11. (a) Histogram of R^2 from sample #01051601; (b) Histogram of RMSE from sample #01051601..... 41

Figure 3-12. (a) Histogram of combined R^2 from all five samples; (b) Histogram of combined RMSE from all five samples..... 41

Figure 3-13. *en face* local retardation and tractographic images of Sample #01051601 obtained at (a, b) 4µm depth; (c, d) 20µm depth; and (e, f) 48µm depth. 44

LIST OF TABLES

Table 3-1. Summary of Cartilage Thickness Measurement 40

IMAGING FIBER ORIENTATION IN ARTICULAR CARTILAGE USING OPTICAL POLARIZATION TRACTOGRAPHY

Xuan Yao

Dr. Gang Yao, Thesis Supervisor

ABSTRACT

Articular cartilage plays a vital role in providing a low-friction surface between the bones of joints. This mechanical function is highly related to the special collagen organization in cartilage, especially in the superficial zone. The “split-line” method has been previously used to examine the fiber orientation in superficial zone of the cartilage. Because the “split-lines” are created by pricking the cartilage surface using a needle, this method is destructive and cannot be used for diagnosis purpose.

In this thesis research, I applied optical polarization tractography (OPT) to visualize fiber orientation in cartilage. OPT is a recently developed high resolution imaging technology based on polarization-sensitive optical coherence tomography. OPT has been previously applied to visualize fiber structures in muscles. We showed that OPT can non-destructively image the fiber orientation in cartilage. The orientation obtained in OPT agreed very well with the split-line results. In addition, the thickness of cartilage and the thickness of superficial zone can be obtained in OPT results. These findings show that OPT has a great potential in clinical orthopedic applications.

Chapter 1. Background and Introduction

Cartilage is the stiff but flexible tissue that connects the joints in bones, the ear, nose and trachea. There are three different types of cartilage found in the body: articular or hyaline cartilage, fibrocartilage, and elastic cartilage. Elastic cartilage contains elastic fiber network and collagen fibers which exists in outer ear and epiglottis. Fibrocartilage consists of fibrous bundles of collagen and it is found in intervertebral disc and meniscus. And Hyaline cartilage is the type of cartilage found in joint, which is mostly made up of type II collagen and chondroitin sulfate. Healthy articular cartilage supports the daily motion, provides less friction between joints and can alter its properties in response to differences in loading. [1]

1.1. Articular cartilage

Although the thickness of articular cartilage is usually only a few millimeters, it has powerful stiffness in response to compression, which helps to protect the subchondral bone by minimizing the peak stress. [2] Articular cartilage consists of highly specialized cells called chondrocytes. It synthesizes collagens, proteoglycan and non-collagenous proteins, and organize them into an ordered matrix, [3] which is the source of its remarkable mechanical properties.

The composition and morphology of the collagen matrix vary over depth from

the cartilage surface. It can be divided into four zones, superficial zone, transition zone, middle zone and calcified cartilage zone. The boundaries between zones can't be accurately defined, but their functional differences are distinct. [2,3]

A thin film of synovial fluid, the 'lamina splendens', exists at the cartilage surface. It provides the gliding surface and reduces friction between joints. Some studies define it as the first layer in the superficial zone. [2] Beneath this thin film, flattened ellipsoid chondrocyte cells lie parallel to the cartilage surface. These chondrocytes synthesize a high concentration of collagen fibrils and organize them into a matrix, which gives the superficial zone greater tensile stiffness and shear strength than deeper zones. Although the superficial zone is the thinnest layer among all four zones, it provides the most important mechanical property with the unique structure and composition.

The transition zone, as the name indicates, connects the superficial zone with the middle zone with an intermediate matrix composition. Spheroidal shapes of cells synthesize the matrix with larger diameter collagen fibrils and higher concentration of proteoglycans but lower concentration of collagens than superficial zone. The middle zone has collagen fibrils of the largest diameter and has the highest concentration of proteoglycans. In the middle zone, the spheroidal chondrocytes are arranged perpendicular to the cartilage surface. [3] Last, the calcified cartilage zone separates the middle zone with subchondral bone.

Microscopic examination shows that articular cartilage lacks blood vessels, lymphatic vessels or nerves. It has a lower level of metabolic activity than regular tissues like muscle, which means it has limited potential to regenerate. This property of

articular cartilage makes any damage or injury irreversible.

1.1.1.Osteoarthritis: diagnosis and treatment

For the middle-aged and older people, joint pain is the primary cause of disability, which usually results from degeneration of the cartilage due to osteoarthritis. [1] Osteoarthritis (OA) is the most common disorder of articular cartilage and can be resulted from progressive cartilage degeneration. Multiple risk factors for the development of OA have been identified, including aging, prior joint injury, genetic factors, synovial inflammation and mechanical influences.[4] The risk of progressive cartilage degeneration increases with aging; meanwhile any old injuries can also eventually result in osteoarthritis.[5]

Because cartilage damage is irreversible, there is a great clinical need for early diagnosis and treatment of cartilage degenerative processes. [6] The earliest microscopic alteration in cartilage degeneration is found in the superficial zone. Localized fibrillation and disruption of the superficial layer are identified as the first signs. [2] The superficial layer of cartilage becomes thinner and eventually completely wears away in osteoarthritis. Studies have revealed increased tissue hydration, disorganization of the collagen network, and a decrease in the tensile stiffness from the superficial layer in the early osteoarthritis. [5] The disruption or remodeling of this superficial zone significantly affects the overall mechanical response of the cartilage and contributes to the progression of osteoarthritis. [6]

Autologous osteochondral transplantation (AOT) has become a promising way to

repair large cartilage damage. [7] In this treatment, osteochondral plugs are obtained from non–weight-bearing areas of the knee joint to an area of cartilage damage. [8] The outcome of this technique may be negatively affected by a poor patient selection (valgus knee mal-alignment, degenerative lesions) or technical problems (size of the graft and mismatch of donor-graft contours). [9]

In AOT, it is important to align the collagen orientation in the osteochondral grafts with the host site. [10] A proper alignment of collagen fibers would minimize the abnormal stress on the cartilage plugs and maximize their long-term viability. [5] In addition, selecting a proper cartilage thickness is also crucial for a better treatment outcome. Zeissler et al [7] concluded that osteochondral transplants should be implanted to match the "split-line" orientation and match the thickness of the grafts with that of the injured cartilage. Therefore, it is important to characterize the fiber orientation and cartilage thickness to ensure a successful transplantation and prevent the early graft degeneration.

1.1.2. Cartilage imaging

Imaging methods are important for osteoarthritis diagnosis and management. Various imaging modalities have been applied for the diagnosis for osteoarthritis, such as magnetic resonance imaging (MRI) and ultrasound (US). [11] However, the spatial resolution in US and MRI is insufficient for detecting the tiny different characters in the early stage of OA. Similarly, although X-ray CT and MRI have been applied to measure cartilage thickness, their resolution cannot resolve the superficial cartilage. [12]

More importantly, no practical methods are available for imaging the orientation of collagen fiber. The “split-line” method has been applied by many groups to investigate the fiber orientation in superficial cartilage. [13,14] However, this method is destructive and is not practical for disease diagnosis and treatment management.

Optical coherence tomography (OCT) has emerged as a promising imaging tool for cartilage. OCT is non-invasive, fast, and can achieve high-resolution. In addition, polarization-sensitive optical coherence tomography (PS-OCT), an extension of OCT, offers additional benefit of being able to imaging collagen fibers. PS-OCT system has the potential to image both cartilage morphology and collagen structure.

1.2. The “split-line” map of cartilage

It is important to evaluate the collagen network structure in the superficial zone because it plays a critical role in normal cartilage function. The ‘split-line’ method provides a simple and effective way to reveal fiber orientation on the cartilage surface. [13]

1.2.1. Creation of split-lines

Split-lines are the cracks created on the articular cartilage surface when pricking the cartilage using a needle. These cracks are caused by the collagen fibers splitting along the lines of tensile stress. To better visualize these cracks, the needle is usually dipped in India ink before pricking, which stains the exposed cartilaginous matrix and makes the split-lines visible. The “split-lines” are similar to Langer’s lines, which are

reflective of lines of tension in the skin. [13]

Meachim et al. [15] is one of the first several groups who studied on split-lines. They tried different metal pins with different tip. And the split lines show different patterns with those different pins and on different location of cartilages.

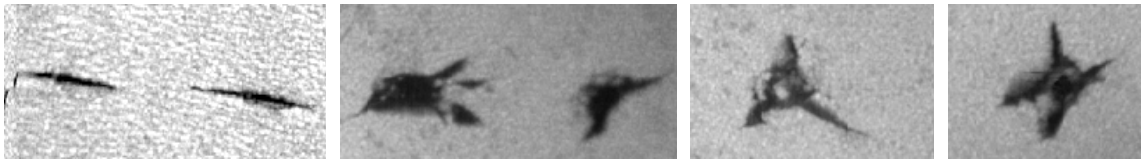

(a) (b) (c) (d)

Figure 1-1. Different split line patterns observed in our study. (a)Straight split line; (b) Curved split line; (c) Sharply angled, forked split line; and (d) Stellate split line.

The split lines produced by a round object were nearly always typically straight and un-branched when examined *en face* (Figure 1-1(a)). Some split-lines may have a curved (Figure 1-1(b)), sharply angled, forked (Figure 1-1(c)), stellate (Figure 1-1(d)) or other atypical appearance when needles were not properly used. The length of different split-lines varies from 0.9 to 1.9 mm when created using a 0.5 mm diameter pin. The different split-line patterns from our test are similar to those observed by Meachim et al. [15]

1.2.2. Interpretation of split-lines

Petersen et al [16] confirmed that the direction of the split lines depends on the orientation of the collagen fibrils in the superficial lamellar layer, which was revealed by scanning electron microscopy (SEM). They prepared a menisci sample in the 4% formalin. In order to expose the entire meniscus cross section, the tissue was removed

layer-by-layer with delicate dissecting instruments and chemical maceration method. [16]

The SEM results [16] showed that the collagen fibrils run parallel to the split lines in the external portions. Non-parallel split-lines were observed due to fibrils intersecting. No distinct split line was produced in areas where the fibril lamellae intersected at right angles. [16]

However, the 'arcade-like' path or the bending trend of the collagen fibrils described in the literature cannot be confirmed by either the scanning electron microscopy or the split lines. [16]

Previous studies [17] showed that the distinct fiber orientation on joint cartilage surface and the structural preference were directly related to the directional variation in stiffness and strength characteristics of the tissue. It is reasonable to assume that in order to best resist the tensile forces produced during the motion or for weight bearing, there will be a unique fiber orientation for different cartilage surface.

Below et al. [18] confirmed that there was a preferential orientation of the collagen fibers in the superficial layer of articular cartilage. And the result from mechanical test verified that cartilages were significantly stiffer and stronger when specimens were tested in a direction parallel to the split line pattern than those were tested perpendicular to the split-line pattern.[18] This is an indicator that if the osteochondral grafts transplanted with the improper alignment, the possibility of failure may increase significantly.

During the progress of osteoarthritis, fibrillation of superficial collagen happens.

This may change the superficial collagen fibril patterns, which can appear as abnormal split-lines. This was demonstrated in the study conducted by Mononen et al [19] using a 3D finite element model. The model was constructed based on magnetic resonance imaging result. In the model, the collagen fibrils resisted strains along the split-line directions. In the normal, intact cartilages, split-lines were oriented into the anterior–posterior direction. However, in the weight bearing area of the osteoarthritis cartilage, split-lines showed a random pattern. [19,20] These findings suggest that normal split-line pattern is the most ideal for prevention of excessive strains that could lead to tissue damage. [19]

1.3. Imaging based on optical coherence tomography (OCT)

OCT is an emerging technology for cartilage imaging. OCT is a non-invasive optical imaging technology. It can produce high-resolution, three-dimensional images in tissue samples in vivo and in real time [21]. OCT is based on measuring the backscattered light from transparent or turbid tissue using optical interferometry (Figure 1-2). Based on the principle of interference, the incident light is split into two separate directions after the beam splitter, the reference arm and sample arm. Light directed into the sample and backscattered in the sample arm, incident light reflected back from the optical mirror in the reference arm. Then the two rays interfere with each other and light back reflected by tissue will be detected collected by photo detector, and then these data are calculated into images.

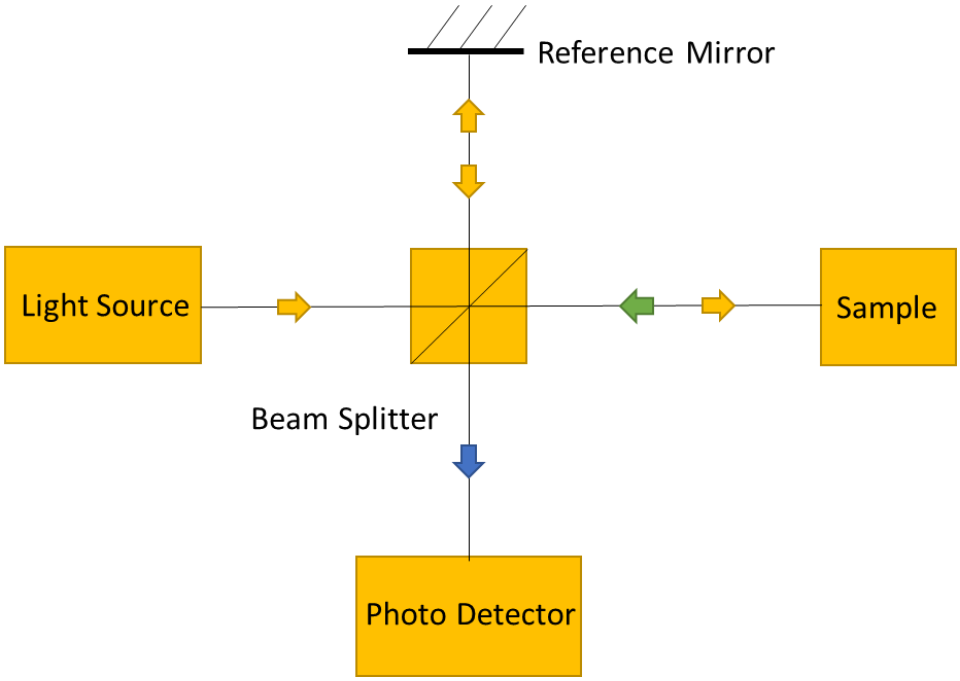

Figure 1-2. A schematic diagram of the OCT system. In Fourier domain OCT, the A-scan is obtained using direct Fourier transform of the interference signal.

In OCT, near-infrared (NIR) light is often used as the light source since it can provide a larger imaging depth. [22] NIR light is within the biological spectral window, so the effect of tissue absorption is minimal. In addition, tissue scattering is also smaller in wavelengths of 800-1300nm than at the visible wavelengths. Therefore, the penetration depth is higher at NIR wavelengths, which enables the system to obtain depth information as much as it can. [23]

1.3.1. Polarization Sensitive Optical Coherence Tomography (PS-OCT)

Although OCT allows non-invasive, high-resolution, cross sectional imaging of tissue sample, the image contrast is merely based on the reflected intensity. Adding more contrast mechanisms can retrieve more information from the sample. Polarization-sensitive optical coherence tomography (PS-OCT) is an extension to

conventional OCT. PS-OCT can measure the polarization states of backscattered light, and is especially useful for imaging the properties of collagen matrix organization. [24]

1.3.2. Fundamentals of optical polarization

Polarization is an important property of the light. As an electromagnetic wave, the electric field vector of light oscillates perpendicularly to the direction of its propagation. When the direction of this electric field oscillates randomly in time, the light is unpolarized. When the direction of the electric field of light is well defined, the light is polarized. Most natural sources of light are regarded as unpolarized, such as the sunlight. Polarized light can be obtained using a special optical component, i.e. the polarizer.

There are three typical types of polarization states. If the electric field vector of light only oscillates in one single plane, its propagation can be tracked as a line within a plan as shown in Figure 1-3(a). This is referred to as “linear” polarization. If the two orthogonal components of the electrical field are equal in amplitude, but have an exact $\pi/2$ phase difference, the electric field vector follows a circular trajectory in time (Figure 1-3(b)). This is the case of circular polarization. Depending on the rotation direction, it can be further classified as left- or right-hand circularly polarized light.

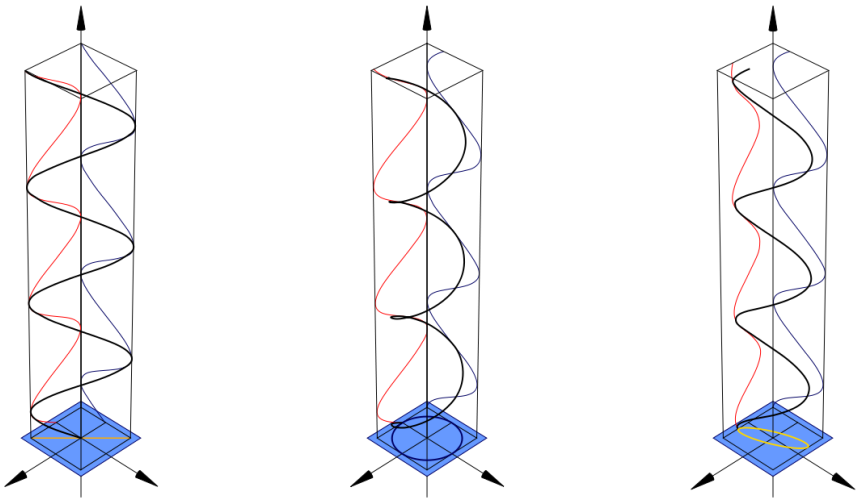

(a) (b) (c)

Figure 1-3. Diagrams of (a) linear polarization, (b) circular polarization, and (c) elliptical polarization. This diagram is from Wikipedia, the copyright holder of this file allows anyone to use it for any purpose.

In elliptical polarization, the electric field vector of light follows an elliptical propagation with time (Figure 1-3(c)). As the elliptical polarization is the most general in the polarized light, the linear and circular polarized light can be viewed as special cases of it.

1.3.3. Jones Matrix description of polarization light

Polarization can be described mathematically with Jones Calculus, developed by R. C. Jones in 1941. [25] He believed that representing light by using electric field vector is the most reasonable way since light is composed of oscillating electric fields.

A polarized light can be represented by a Jones vector defined as

$$\mathbf{E}(t) = \begin{bmatrix} E_x(t) \\ E_y(t) \end{bmatrix} = \begin{bmatrix} E_{0x} e^{i\varphi x} \\ E_{0y} e^{i\varphi y} \end{bmatrix}, \tag{1-1}$$

where $E_x(t)$ and $E_y(t)$ are the instantaneous scalar components of the electric field. For

the horizontal and vertical polarization states, the Jones vectors can be represented as:

$$E_h=\begin{bmatrix}E_x(t)\\0\end{bmatrix} \text{ and } E_v=\begin{bmatrix}0\\E_y(t)\end{bmatrix}. \quad (1\text{-}2)$$

For the right-circularly and left-circularly polarized light, the x and y components have the same amplitude in these two states but with a phase difference of ϕ. For left-circular polarization, the phase of x-component leads the y-component by π/2, while for right-circular polarization the situation reverses.

$$\mathbf{E}=\begin{bmatrix}E_0e^{i\varphi}\\E_0e^{i(\varphi-\frac{\pi}{2})}\end{bmatrix}. \quad (1\text{-}3)$$

The normalized representation for these two states are

$$\mathbf{E}_R=\frac{1}{\sqrt{2}}\begin{bmatrix}1\\-i\end{bmatrix} \text{ and } \mathbf{E}_L=\frac{1}{\sqrt{2}}\begin{bmatrix}1\\i\end{bmatrix}. \quad (1\text{-}4)$$

The polarization properties of an optical material can be described by Jones matrices. The resulting polarization after light crossing the optical element is the product of the Jones matrix of the optical element and the Jones vector of the incident light. For example, the incident light can be defined as $\mathbf{E}_i$, the emerging light after interacting with the optical element is $\mathbf{E}_t$.

$$\mathbf{E}_t=\begin{bmatrix}E_{tx}\\E_{ty}\end{bmatrix}=\mathbf{J}\bullet\mathbf{E}_i=\begin{bmatrix}a&b\\c&d\end{bmatrix}\begin{bmatrix}E_{ix}\\E_{iy}\end{bmatrix}, \quad (1\text{-}5)$$

where **J** is the Jones matrix for that optical element. For example, the Jones matrix of a vertical linear polarizer is $\begin{bmatrix}0&0\\0&1\end{bmatrix}$.

1.3.4. Birefringence

Birefringence is a common polarization property of an anisotropic material,

where the optical refractive index of the sample depends on the direction of light propagation and the polarization state of the light. [26] Birefringence can be found in all fibrous tissues composed by collagen, keratin, such as nerve, muscle and cartilage.

In birefringent materials, a single ray of light can be divided into two beams of different directions based on the polarization and the incident angle. As a comparison, for the isotropic crystal, no matter what direction that light incidents the refractive index is the same.

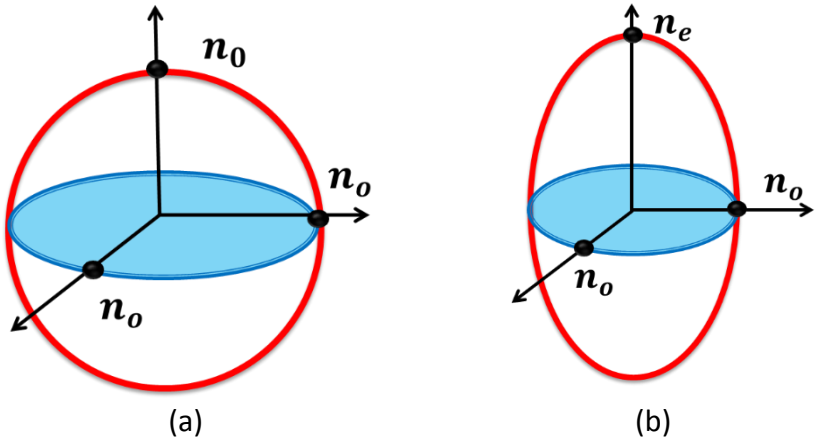

(a) (b)

Figure 1-4. Illustration of (a) Isotropic crystal ($n_1=n_2=n_3=n_0$) and (b) Uniaxial crystal where $n_e \neq n_0$.

Due to the different refractive indices, there are two different axes that light propagates along with a different velocity. If $n_e>n_o$, then the fast axis is along n_o, the slow axis is along n_e. In fibrous tissues, the fiber orientation is usually along the "slow" axis. The amount of "birefringence" of such anisotropic sample is defined as $\Delta n=n_e-n_o$, which can introduce "phase retardation" in the incident light of different polarization states: $\Delta\phi=(2\pi/\lambda)t\Delta n$, where t is the sample thickness and λ is the light wavelength. Both the phase delay and optical axis can be detected in a PS-OCT system. [27]

1.3.5.OCT and PS-OCT imaging of cartilage

Most OCT applications in cartilage are related with the OA early diagnosis. During the course of OA, the superficial cartilage layer is affected first, and irregularities, erosion and fissuring on cartilage surface are considered as earliest signs of OA.

Clinical arthroscopic OCT imaging is one of these applications, which helps the detection of surface fibrillation, cracks and fissures on human cadaver knees in situ [28]. The surface roughness measurement of cartilage can also be measured by the OCT system. [29] Saarakkala et al showed that there is a up to 30 μm difference in roughness between healthy articular cartilage and the OA cartilage. Real time 3D OCT showed superiority [30] in assessing cartilage surface, integrity and homogeneity, and indiscriminating between unmineralized and mineralized cartilage effectively. [31]

As light waves are transverse and can carry polarimetric information, Polarization Sensitive OCT (PS-OCT) is thus able to assess altered birefringence and changes of collagen organization in cartilage. [32]

Li et al. [33] found that there was a depth-resolved banding pattern from normal cartilage while it was lost upon progressive cartilage degeneration. Then Chu et al. investigated the use of PS-OCT birefringence to grade osteoarthritic lesions in human cadaver knees. [34] And Lu et al. [35] reported that conical scan PS-OCT can locate the “brushing direction” (orthogonal to split line direction) of collagen fibers in articular cartilage which might reflect the magnitude and direction of the dominant shear-stress experienced at a particular site during locomotion [36] and might offer valuable

reference for osteochondral autograft transfer.

1.4. Contribution of this thesis research

Although PS-OCT is promising for cartilage imaging, none of the previous studies have been able to image the fiber orientation in cartilage. It is known that the optical axis in a birefringent tissue is related to the fiber orientation. Unfortunately, the optical axis measurement obtained in PS-OCT represents the “cumulative” axis. Such results are affected by all tissues from the surface to the image depth, and therefore do not represent the actual fiber orientation.

Optical polarization tractography (OPT) was recently developed to imaging fiber orientation by extracting “local” optical axis from PS-OCT measurements. [37,38] By combing the optical axis result from PS-OCT system with advanced tractography rendering, OPT is an imaging technology that detect the complicated fiber orientation and visualize it intuitively. OPT has been applied to image fiber structure in skeletal muscle, heart muscle, and blood vessels. In this study, we show that OPT can imaging the fiber orientation in cartilage. The obtained fiber orientation was consistent with the split-line results.

Chapter 2. Experimental Methods

2.1. Optical Polarization Tractography (OPT)

2.1.1. Imaging system

In this study, OPT is implemented in a Jones matrix PS-OCT system which is illustrated in Fig. 2-1. The light source is a super-luminescence diode (SLD) with a central wavelength λ_0 of 847.8 nm and 58.3 nm spectral bandwidth (FWHM). [39,40] The theoretical axial resolution is 5.4 μm in air when estimated using $\Delta x = (2\ln 2/n\pi)\,\lambda 2/\Delta\lambda$. [39]

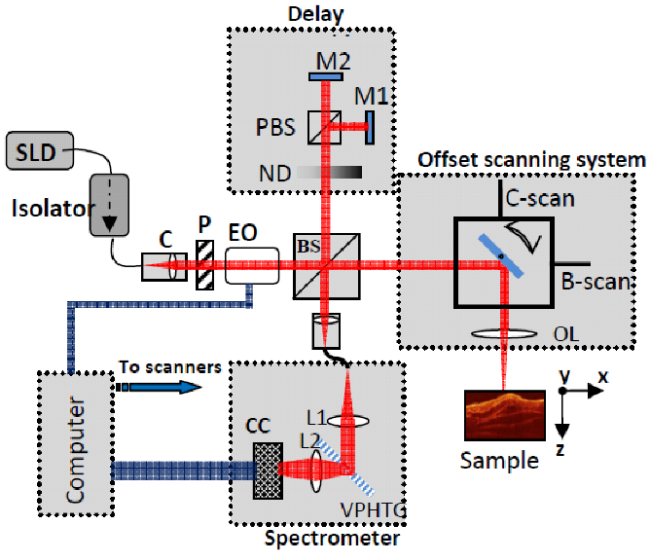

Figure 2-1. A schematic diagram of the PS-OCT system. SLD: Superluminescent diode; C: collimator, P: a polarizer for generating vertically polarized light; EOM: electronic optical modulator; BS: non polarization beam splitter; ND: neutral density filter; PBS: polarization beam splitter; M1, M2: reference mirrors for the horizontal and vertical polarization components; L1: achromatic collimation lens (f = 30 mm); L2 achromatic focusing lens (f = 120 mm); OL: objective lens (f = 60 mm); VPHTG: volume phase holography transmission grating (1200lines/mm).

Light was linearly polarized by the polarizer after emitting from the SLD, traversing through an isolator and being collimated by a collimator (C). The electro-optical modulator (EO) is applied to generate an alternating left-circularly (LC) and right-circularly (RC) polarized light. Then the polarized light was split by a beam splitter (BS) into the reference arm and the sample arm. [39]

In the reference arm the incident light passes through a neutral density filter (ND) and then was split into two beams after passing a polarization beam splitter (PBS). M1, M2 are reference mirrors, as horizontal-polarized light goes to the H mirror, and vertical-polarized light goes to the V mirror. In order to create a delay between the two orthogonally polarized lights, these two mirrors are positioned at a different distance to the PBS. Because of the delay, it is possible to separate the positions of the vertically and horizontally components in depth to obtain the individual information of H and V to reconstruct the image. [40]

In the sample arm, a galvanometer scanner reflected the incident polarized light into an objective lens (OL) which focused the light into the sample. The backscattered light from the sample was recombined with the light backscattered from the reference arm at the beam splitter, then coupled into the spectrometer by the fiber.

Afterwards the recombined light is collimated by an achromatic collimation lens (L1) and diffracted by a volume phase holography transmission grating (VPHTG). Another achromatic focusing lens (L2) images the spectrum into a linear CCD camera.

Three-dimensional image is created by the PS-OCT system with three different scans A, B, C. A-scan gives the information over depth, and multiple A-scans develop a 2-

dimensional image with B-scan, then multiple B-scans are combined to construct the three-dimensional figure. Also the three-dimensional image can be viewed separately in the en-face, cross-sectional, and sagittal plane. In this study, the pixel size in the image was 4.0μm, 4.0 μm, and 4.0 μm along the A, B, and C-scan directions, respectively (z-, y- and x-axes respectively).

2.1.2. Optical Axis Calculation

After system setup and calibration, a sample was imaged using backscattered signals from two orthogonal (horizontally and vertically polarized) components. This was repeated using both right- and left-handed circularly polarized incident light generated using the EO modulator.

Since only the “round-trip” signal can be detected in OCT, conventional PS-OCT measurements are integrated results from the sample surface to the measurement depth. In a birefringent sample, the depth-varying optical axis is not correct with that integrated method. Our method can derive a true depth-resolved local optical axis along with local retardance in conventional PSOCT systems. [41]

As mentioned in the introduction part, polarized light, like vectors, can be described using the Jones vector. And the Jones matrices are operators that represent the sample polarization properties. With birefringent local Jones matrix $\mathbf{J}_L$, a sample segment at a particular depth, the corresponding nth layer (represented as the nth image pixel in the A-scan) can be expressed with tissue polarization properties (local optical axis θ and a complex local retardance $\gamma_n = \delta_L + i\sigma_L$) as

$$\mathbf{J}_n = \mathbf{J}_L(\theta_n, \gamma_n), \tag{2-1}$$

where δ_L is retardance, σ_L is diattenuation. The local birefringence can be calculated as $\Delta n = \lambda\delta_L/2\pi d$, where d is the pixel size.

The sample image was collected in a "planar" 3D matrix of 1024 × 2000 × 1000 pixels in A-, B-, and C-scans, respectively. Jones matrix will be constructed using local δ, σ and θ at each pixel in the image. First, a complex matrix **K**(n+1) was constructed by the measured cumulative round-trip Jones matrices at two adjacent axial pixels:

$$\mathbf{K}(n+1) = \mathbf{J}_L^{-1}(\varphi_n, \kappa_n)\mathbf{J}_{RT}(\mathrm{n}+1)\mathbf{J}_L^{-1}(\varphi_n, \kappa_n), \tag{2-2}$$

where $\mathbf{J}_{RT}$ (n+1) was the directly measured "round- trip" Jones matrix at the $(n + 1)^{th}$ depth layer. The ϕ_n and κ_n here are directly measured from $\mathbf{J}_{RT}$(n), then $\mathbf{J}_L(\phi_n,\kappa_n)$ at n^{th} depth can be derived as:

$$\mathbf{J}_{RT}(\mathrm{n}) = \mathbf{J}_L(\varphi_n, 2\kappa_n). \tag{2-3}$$

The complex local retardance δ_L can be calculated from the eigenvalues of matrix **K**(n+1), then diattenuation σ_L can be removed from $\mathbf{J}_{RT}$(n), which is required for calculating the true local axis result by using only the real component of the measured complex retardation.[41] A modified matrix $\mathbf{J}_{RT}$'(n) was derived as a function of only local retardance and optical axis and a "single-trip" Jones matrix of the $(n - 1)^{th}$ layer calculated from the local retardance and optical axis was derived as $\mathbf{J}_{ST}$(n).

By using eigen decomposition, the local optical axis can be calculated from

$$\mathbf{J}_{LT}^{\mathrm{T}}\mathbf{J}_L = \left[\mathbf{J}_{ST}^{\mathrm{T}}\mathbf{(n\text{-}1)}\right]^{-1}\mathbf{J}'_{RT}(\mathrm{n})[\mathbf{J}_{ST}\mathbf{(n\text{-}1)}]^{-1}. \tag{2-4}$$

The above procedure was iteratively computed starting from the sample surface where the local Jones matrix and the single-trip Jones matrix were the same. [37]

In OPT the obtained local axis, which is tracked between [–90°, 90°] with zero degree aligned with the C-scan direction (x-axis) and fiber orientation was visualized with streamline function in MATLAB. From the intensity data, a sample surface boundary was detected using a threshold-based segmentation program. Then collecting all pixels at a given transmural depth created an *en face* image; and combining all *en face* images formed the 3D fiber tractography.

2.2. Split-line generation and analysis

In order to generate consistent split lines, a needle was inserted at 90° to the cartilage surface until reaching the subchondral bone. This causes the collagen fibers of the superficial layer of the cartilage to split along their lines of tensile stress. Before insertion, the needle was dipped in commercial grade India ink, which stained the exposed cartilaginous matrix, making the split lines clearly visible. [13] The results of split-line pattern from all samples were photographed using a digital camera. After the OPT tests, all the samples were fixed in the formalin solutions for histology analysis.

2.2.1. Needle Choice

To obtain the clearest pattern of split line, several different needles were tested. First, we tried the injection needle (BD PrecisionGlide™ Needles, #305176, 20 G x 1 1/2 in). It gave a pretty clear split line pattern (Figure 2-2 (a)), however, the orientation of split line it created was not reliable due to the injection tip. Specifically the split-line orientation was affected by the direction of needle tip (Figure 2-2 (b)).

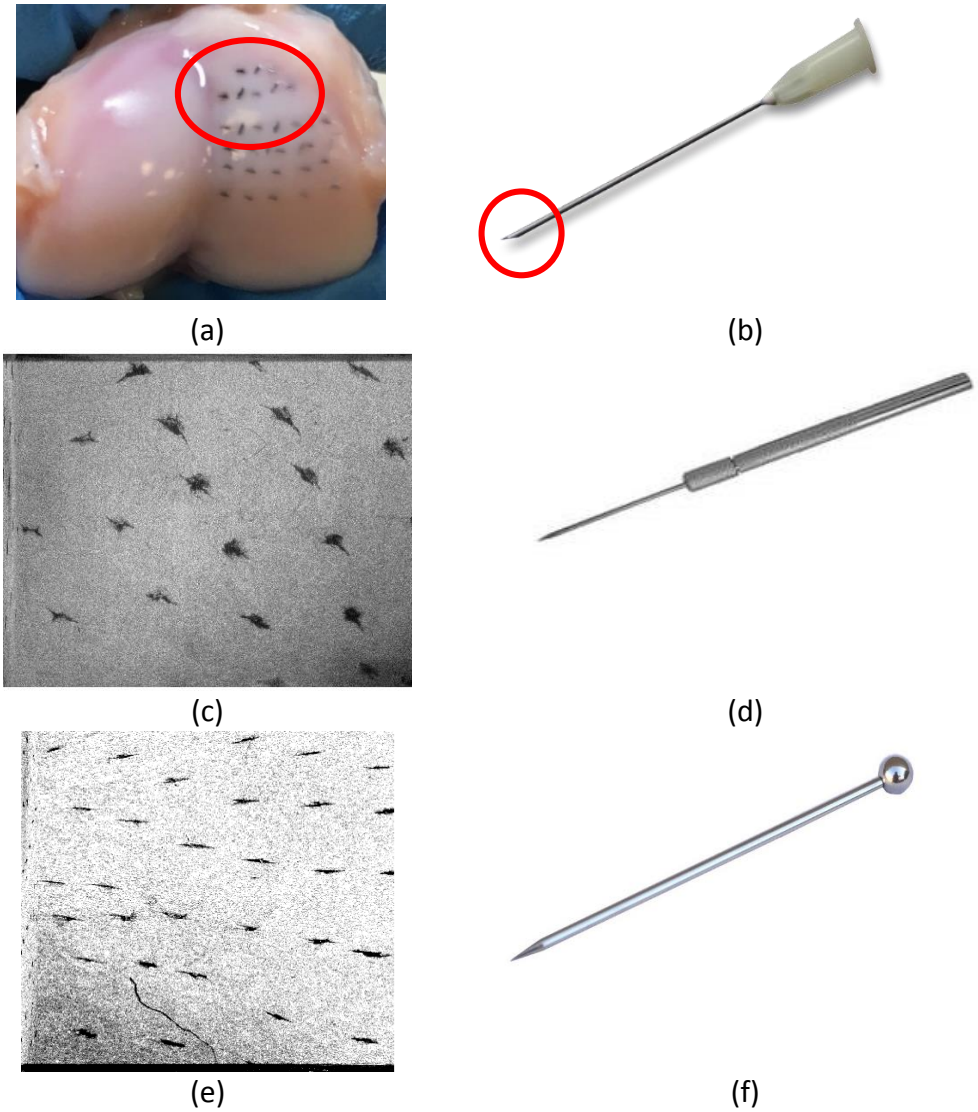

Figure 2-2. (a) Split line patterns created by injection needle with two perpendicular directions. (b) Example image of injection needle with tip (red circled area). The orientation of split line changes with the alteration of tip direction (red circled part). (c) Intensity image of split line pattern created by dissecting needle; (d) Example image of dissecting needle. (e) Intensity image of split line pattern created by conical needle with fine tip; (f) Example image of conical needle with fine tip.

The dissecting needle was also tested (Figure 2-2(d)). It can avoid the unreliable problem as in injection needle because of its symmetric tip. However, the tip of dissecting needle is not fine enough (diameter: 1.2 mm). When pricking the sample with

ink, there will be too much ink immersing into the hole, which results in an undistinguishable quality of pattern.

Finally, we found the conical needle (Dritz® long ball point pins, #16950, 1-1/2 in (38 mm) with fine tip (diameter: 0.62 mm) (Figure 2-2 (f)) was the best to produce split-lines. The patterns of split line it created are distinguishable and stable. The quality of split line pattern will directly affect the accuracy of calculation for split line orientation and the goodness of line fitting, which represents the reliability of our line fitting method.

2.2.2. Split line images and quantification

After the split line pattern was ready, sample was attached to a stage with a rubber substrate which can make it stable while tilting the stage. In order to align the sample to the focal plane and perpendicular to the incident light, the stage was adjusted in all three directions. The OCT signal was monitored while adjusting the sample mounting. Until the surface was adjusted into a best position, the cross-section pattern showed a clear shape of cartilage without overlapping between H and V components, the sample was ready to be scanned.

In this study, the articular cartilage sample was scanned with a total of 1000 B-scans and constructed a 6.0×6.0×1.0 mm^3 volume (2000×1000×293 pixels along Y-X-Z-directions) (2000 pixels in each B-scan covering 6.0 mm). The entire scanning took 80 seconds to complete. The images were resized using cubic spline interpolation to adjust the pixel size into 4.0μm along all dimensions.

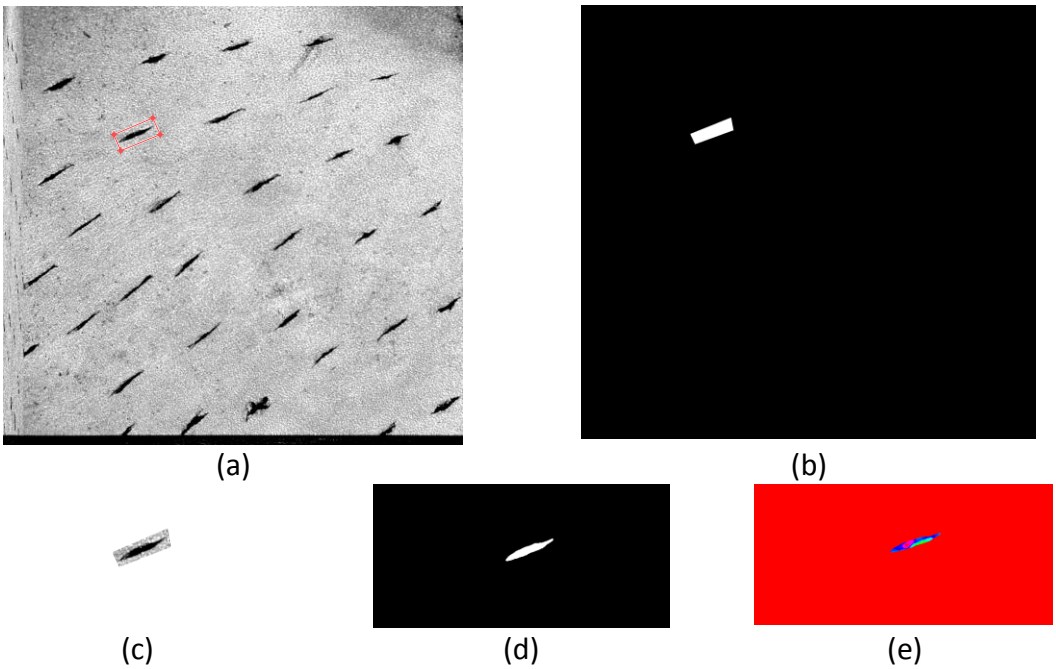

Figure 2-3. Illustration of procedures of fitting: (a) Choose ROI from *en face* intensity image; (b) Create a binary image of ROI; (c) Get the greyscale image of ROI and extract split line in ROI; (d) Get the split line binary mask; (e) Get the equivalent area from optical axis image, represented with HSV colormap.

A line-fitting program was developed and applied to the intensity image to calculate the angle of each split line. General procedures are illustrated in Figure 2-3. With this program, we chose a split line region of interest (ROI) from *en face* intensity image, and saved as a binary image.

Then split line can be extracted with a small greyscale image by multiplying the binary ROI image with the original intensity image. As in the small greyscale image, the split line is darker than the background, a threshold was set to separate the pixel dots in split line from the background and saved them as a binary mask. To increase the quality of fitting, the intensity image was averaged from the 40μm (10th layer) to the 240μm (60th layer). Also the contrast of intensity image was adjusted using imadjust function in MATLAB by setting the intensity range from 0.3 to 0.6.

The orientation of each split line was calculated by fit function and was saved into a data set. After obtaining the angle from split line, it is necessary to know the goodness of fitting. The fitting model applied here is the linear polynomial model, curve(x)=slope*x+intercept. The fitted result includes the several parameters indicating the goodness of fitting as mentioned above. Basically the R-squared (coefficient of determination), Root mean squared error (standard error) are the most common parameters for evaluating the fitting.

In statistics, the coefficient of determination is a number that indicates how well data fit a statistical model. An R^2 of 1 indicates that the regression line perfectly fits the data, while an R^2 of 0 indicates that the line does not fit the data at all.

The root-mean-square error (RMSE) is a frequently used measure of the differences between values (sample and population values) predicted by a model or an estimator and the values actually observed. As the R-squared and RMSE were saved into excel sheet, it is easy to get the distribution of them for evaluation.

For example, the results for the illustrated example split line (Figure 2-3) are listed below.

curve (x)=slope*x+intercept

Coefficients (with 95% confidence bounds): slope=0.42 (0.41, 0.43)

Goodness: R^2=0.95; RMSE=2.13 pixel

2.2.3. Correlation between split line OPT

Once all split lines were segmented, their locations were stored as image masks.

These “split-line” masks were multiplied with the fiber orientation image obtained in OPT. Therefore all images pixels with OPT axis information were collected at each split line (Figure 2-3 (e)). Then the OPT fiber orientation at each split line was calculated by circular average:

$$\theta_L = \frac{1}{2}\tan^{-1}\left(\frac{\langle \sin 2\theta_p \rangle}{\langle \cos 2\theta_p \rangle}\right) \quad (2\text{-}5)$$

where θ_p is the local fiber orientation for each pixel. $\langle \sin 2\theta_p \rangle$ and $\langle \cos 2\theta_p \rangle$ were averaged over the predefined ROI. [38]

The above calculation was repeated for the OPT images obtained at all depths. At this point, the orientation angles of split lines were obtained from both the intensity split line image and the OPT images. Correlation analysis was then carried out to compare these two measurements.

Chapter 3. Results and Discussions

In this chapter, we described and discussed the results of split-line measurement in cartilage and its comparison with OPT results. The line fitting method used for quantitative split-line characterization was also evaluated.

3.1. Cartilage samples

We measured five areas from three different cartilage samples. We obtained porcine articular cartilage from fresh pig foot bought from local supermarket (Moser's Discount Grocery, Columbia, MO). After dissecting the pig foot, the sample cartilage from the first phalanges was obtained. Synovial fluid was present in all articular cartilage samples. The phalanges location was chosen for its relatively flat surface. A smooth flat specimen surface makes it easier to align image planes and achieve the same resolution over the whole sample.

Figure 3-1. Photo of dissected cartilage sample from the first phalanges in pig foot.

3.2. Top Scan Intensity image and split line fitting

Figure 3-2 shows an example result of the split-line pattern, OCT intensity image, and the line-fitting result of the split-lines.

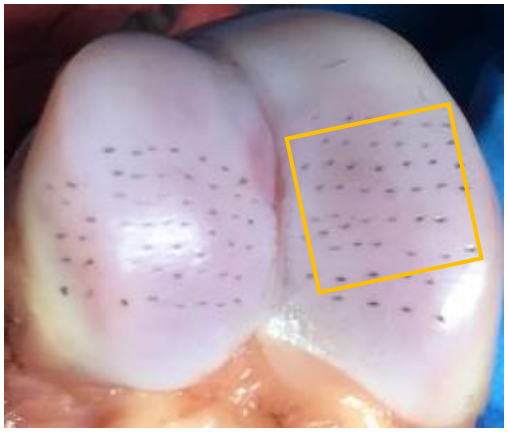

(a)

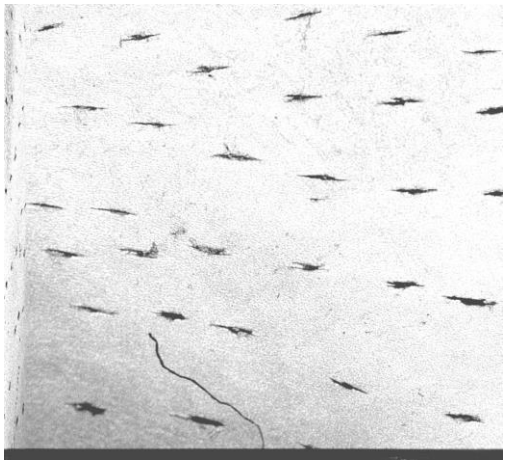

(b)

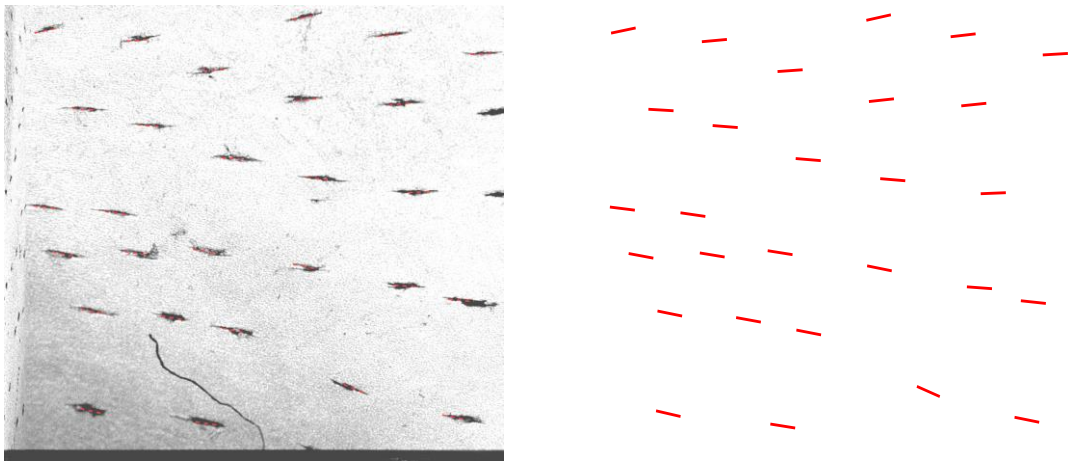

(c) (d)

Figure 3-2. (a) Articular cartilage from pig first phalanges with split line patterns. Yellow square area (6*6mm) was scanned on sample #0105161; (b) *en face* intensity image of sample; (c) Fitting result plotted over the intensity image with a red dashed line; (d) Fitted split line plot with a white background.

After generating the split line with needle, the sample was imaged using OPT. The image covered a 6×6 mm^2 area. The Figure 3-2(b) shows an example OPT intensity image obtained with the averaged intensity method which is mentioned in the section 2.2.2. It is clear to see every split line. The pattern of split line doesn't change over depth. In order to verify that the optical axis result measured by OPT is consistent with the split lines, we need the split line orientation first. With our line fitting method split line was chosen one by one, for this sample there were totally 28 split lines. The angles of all split lines were saved for further correlation studies. The fitting result was drawn on the intensity image with red dashed line. The fitted lines represent the orientation of split line well.

3.3. Fiber orientation from optical polarization tractography (OPT)

Then we checked the optical axis result from OPT and the result was visualized with the

streamline function in MATLAB as shown in Figure 3-3. The optical axis image from transmural depth 48µm. All the depths mentioned below are the transmural depth, which is the depth from the sample surface. It was plotted with the colormap hsv in a range from -90° to 90°, as illustrated in the color bar. As shown in the axis image, the color changes from green to light blue, the angle range is from -20° to 10°, major part of this axis is in the range -10° to 5°.

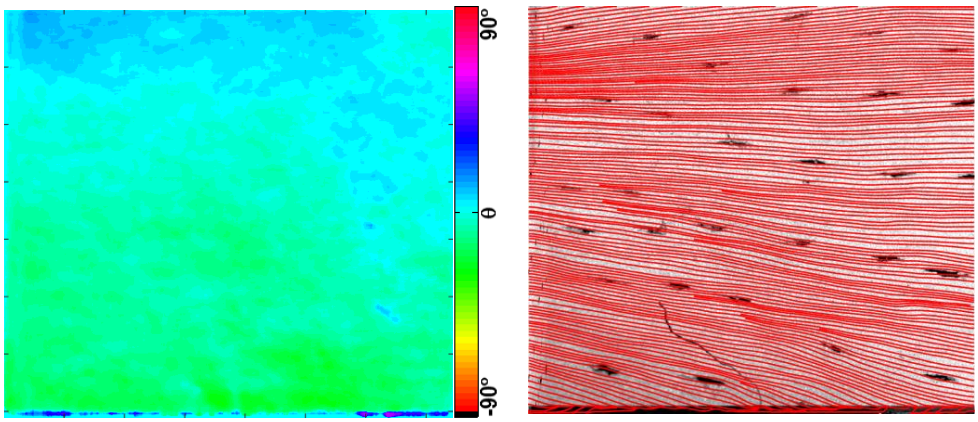

(a) (b)

Figure 3-3. (a) *en face* axis image from depth of 48µm. Axis was shown in hsv color ranging from -90° to 90°. (b) The streamline plotted overlaid on the intensity image.

In the method chapter, it has been described that the axis of split line region can be obtained with the fitting program simultaneously and the angle of each split line region was also obtained (Figure 3-3).

3.4. Correlation Analysis

Once the fiber orientation was obtained using both split-line and OPT, we can compare them using the correlation analysis. The OPT result was plotted vs. Split line result in Excel, and the best correlation achieved at 48µm to 72µm depth as shown

below (Figure 3-4 (a-d)). The coefficient of determination (R^2) and standard error (RMSE) were calculated during the correlation (Figure 3-4 (e-f)). By plotting these two parameters with depth, the variation of correlation over depth is clear.

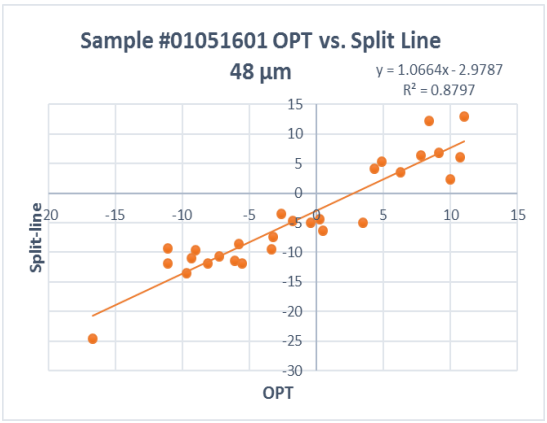

(a)

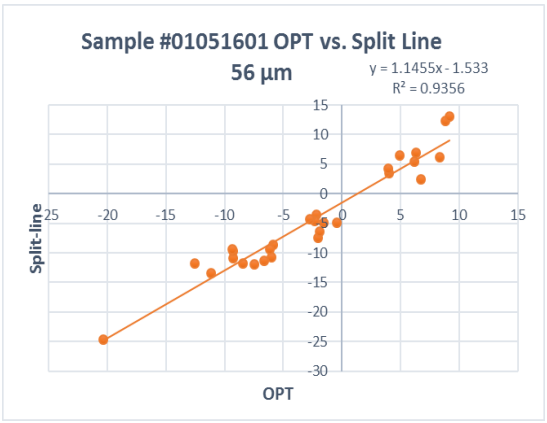

(b)

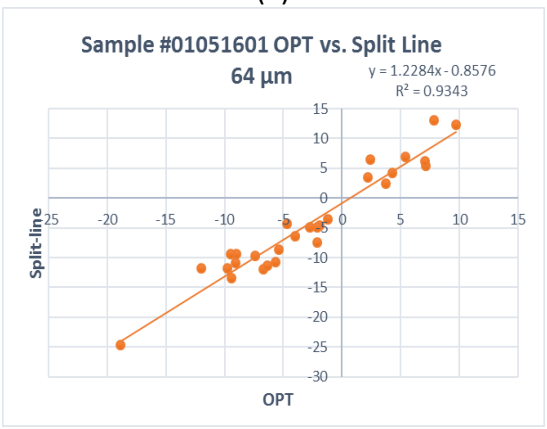

(c)

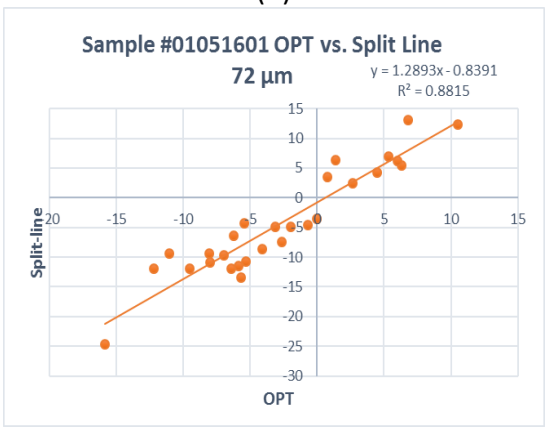

(d)

(e)

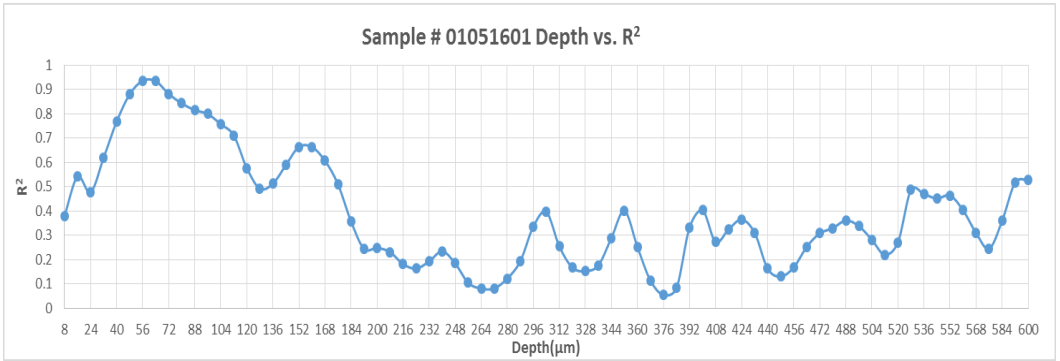

(f)

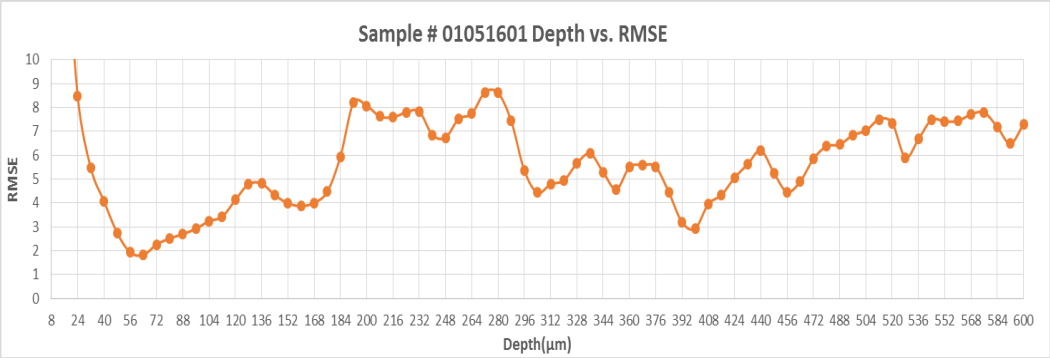

Figure 3-4. Correlation curve of sample 01051601 (OPT vs. Split Line). (a) Correlation curve at 48μm; (b) Correlation curve at 56μm; (c) Correlation curve at 64μm; (d) Correlation curve at 72μm; Correlation analysis result of sample 01051601 (0-600μm). (e) Distribution of R^2; (f) distribution of RMSE.

From depth 0 to 200μm, which is a possible thickness range for superficial zone, R^2 increases from 0.4 at depth 8μm to 0.93 at depth 56μm. At depths deeper than 120μm, R^2 decreases to 0.57 and stays under 0.7. The distribution of RMSE shows an opposite, but consistent pattern as the distribution of R^2. At depths from 40 to 112μm, the value of RMSE stays under 3 pixels which indicates a good correlation. At depths deeper than 112μm, the value of RMSE increases, suggesting a large variation between the optical axis result and split line. After 200μm the variation shows fluctuation like noise without a clear trend. This result is equivalent with the previous studies that the split line represents the fiber trend in superficial zone where the fiber is parallel to the cartilage surface.

As in the example sample (# 01051601), almost all the fiber orientations are in a relatively small range (-10° to 10°) which may be not convincible enough as a proof that the OPT can visualize fiber trend and correlated highly with split line. Therefore, the result of # 01241602 is shown in Figure 3-5 as an addition proof of reliability of OPT method.

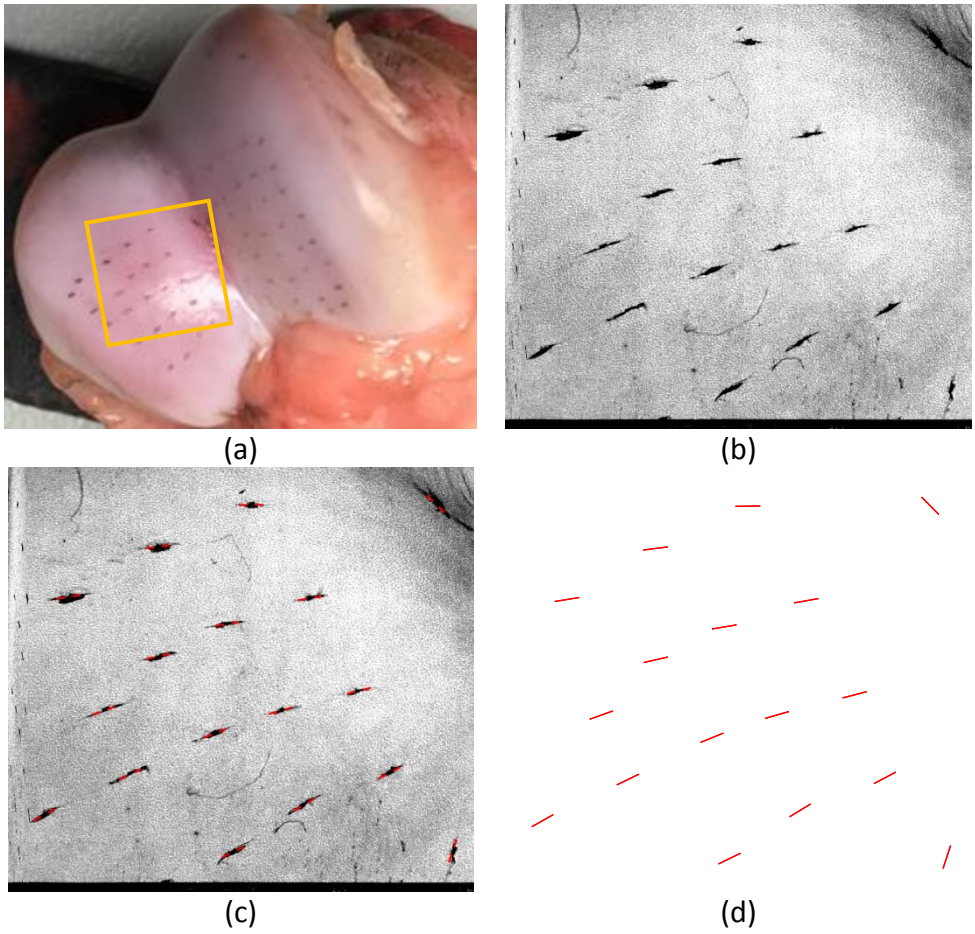

Figure 3-5. (a) Articular cartilage from pig with split line patterns, yellow square area (6*6mm) of sample #01241602; (b) *en face* intensity image of sample; (c) Fitting result plotted over the intensity image with a red dashed line; (d) Fitted split line plot with a white background.

It is clear that from the *en face* intensity image of sample #01241602, two split lines at the two corners (right top and bottom) have a large difference in orientation from other split lines in the middle of the sample. And the line fitting result shows the angles of these two lines are -45.86° and 72.21° respectively while the orientation of the majority lines ranged from 15° to 30°. Then we check the optical axis result with streamline to see the correlation result generally.

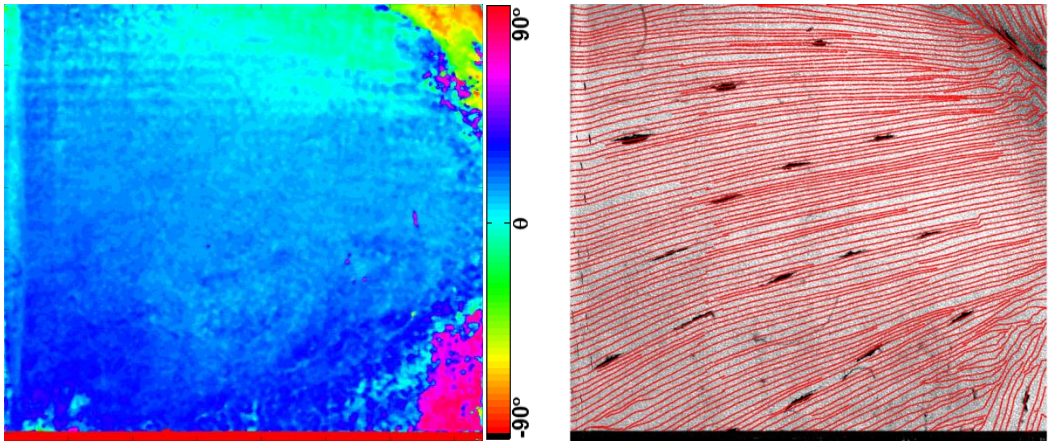

(a) (b)

Figure 3-6. (a) *en face* axis image from another sample #01241602 at depth of 48µm; (b) streamline plotted over intensity image.

From Figure 3-6, it is easy to tell that not only the majority of split lines have the almost the same orientation with optical axis, these two cornered split lines with large difference in angle are also aligned with streamline, which indicates that the fiber orientation in *en face* plane is inhomogeneous at the same depth. As the sample image shown in Figure 3-6, these two split lines are closer to the "groove" of the whole cartilage, which may provide an explanation for their different orientations. With this additional proof, the optical axis from OPT method was in good agreement with the split-lines.

3.5. Best Correlated Depth

After checking the correlation curve throughout five tests, we found that the best correlation was achieved at depth 48-72µm. By combining all results from five samples at depth 48µm, 56µm, 64µm and 72µm the correlation curve was created and shown below.

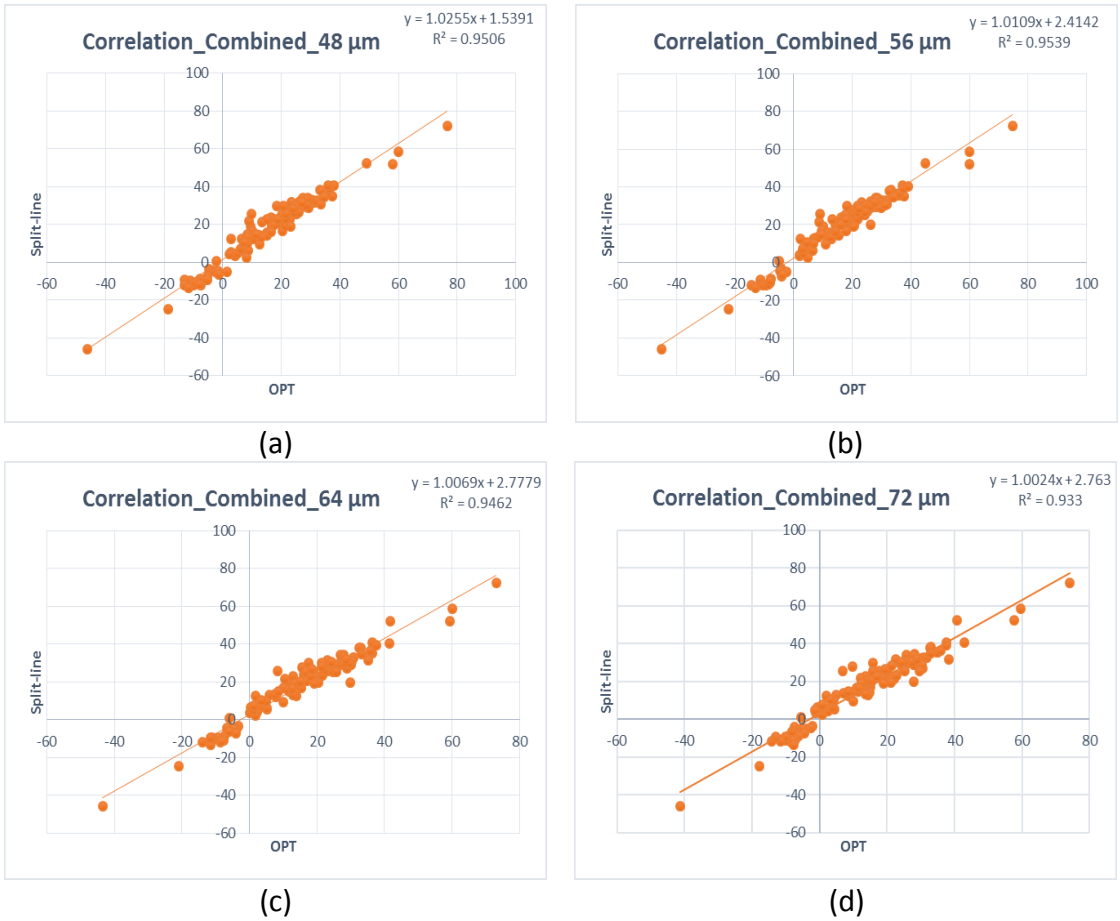

Figure 3-7. Correlation results from five different cartilage samples at (a) depth 48µm with 0.9506 as value of R^2 and 1.0255 as value of slope; (b) depth 56µm with 0.9539 as value of R^2 and 1.0109 as value of slope; (c) depth 64µm with 0.9462 as value of R^2 and 1.0069 as value of slope; (d) depth 72µm with 0.933 as value of R^2 and 1.0024 as value of slope.

The slope from the combined correlation curve is around 1.01 and a 0.95 coefficient of determination suggests a strong correlation. Therefore, these results indicate that OPT is a reliable method that can replace the split line method to evaluate the fiber orientation in the superficial zone of articular cartilage.

3.6. Thickness measurement from Top Scan

Previous studies show that the retardation in articular cartilage is a function of

tissue depth. The retardation curve which was plotted over depth, shows two peaks pattern. Because of the relatively high concentration collagen and thick fibrils in superficial zone then turning to less organized and sparsely distributed in transitional zone, the width of the first peak of retardation curve represented the thickness of superficial zone. And the tide mark of cartilage can be represented by the onset the second peak which is observed by Arokoski et al. [42,43,44].

The local retardation profile from OPT top scan also achieved the similar two-peak pattern as shown in Figure 3-8.

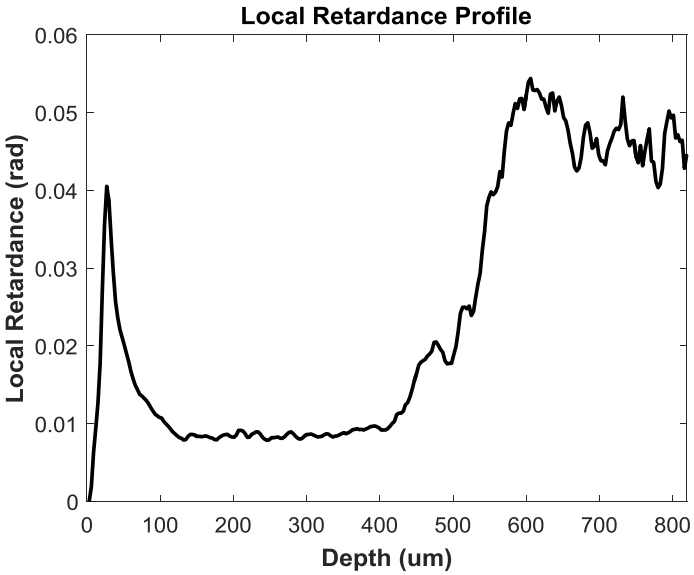

Figure 3-8. Local Retardation averaged from one cross-section from middle of the sample image plotted over the depth in sample #01051601

Since this profile of retardation is from OPT top scan, it shows some different features with Polarized Light Microscopy result from Xia et al. [44] In OPT top scan, light incidents perpendicularly to the surface of cartilage, which will first generate the

relatively large delay, the retardation, due to the parallel arrangement of fibrils in the superficial zone. Then retardation will decrease and stabilize in the transitional zone and the middle(deep) zone. Such a depth profile enables us to roughly measure the thickness of cartilage and superficial zone. Here from the local retardation profile which was averaged from one cross-section image from middle of the sample, the thickness of superficial zone is 120μm, and thickness of cartilage is 580μm.

3.7. Discussions

As mentioned above, the correlation between optical axis result and the split line changed with the depth in the cartilage sample. Previous studies [45] revealed that there is a unique 'arcade' like architecture in articular cartilage and split line just represents the predominant fiber trend in superficial zone. In order to verify these and the thickness measurement from top scan, we scanned the sample from side and did the histology to directly look at the fiber structure over depth.

3.7.1. Scan the sample from side

The cartilage sample used for #01051601 was decalcified for 24 hours after optical imaging. It was then cut along the split line into a small piece (Figure 3-9 (a)). Mark 1 on the sample indicates the left part is the sample #0105161, we just scanned the left part with a 6×6mm^2 area for validation.

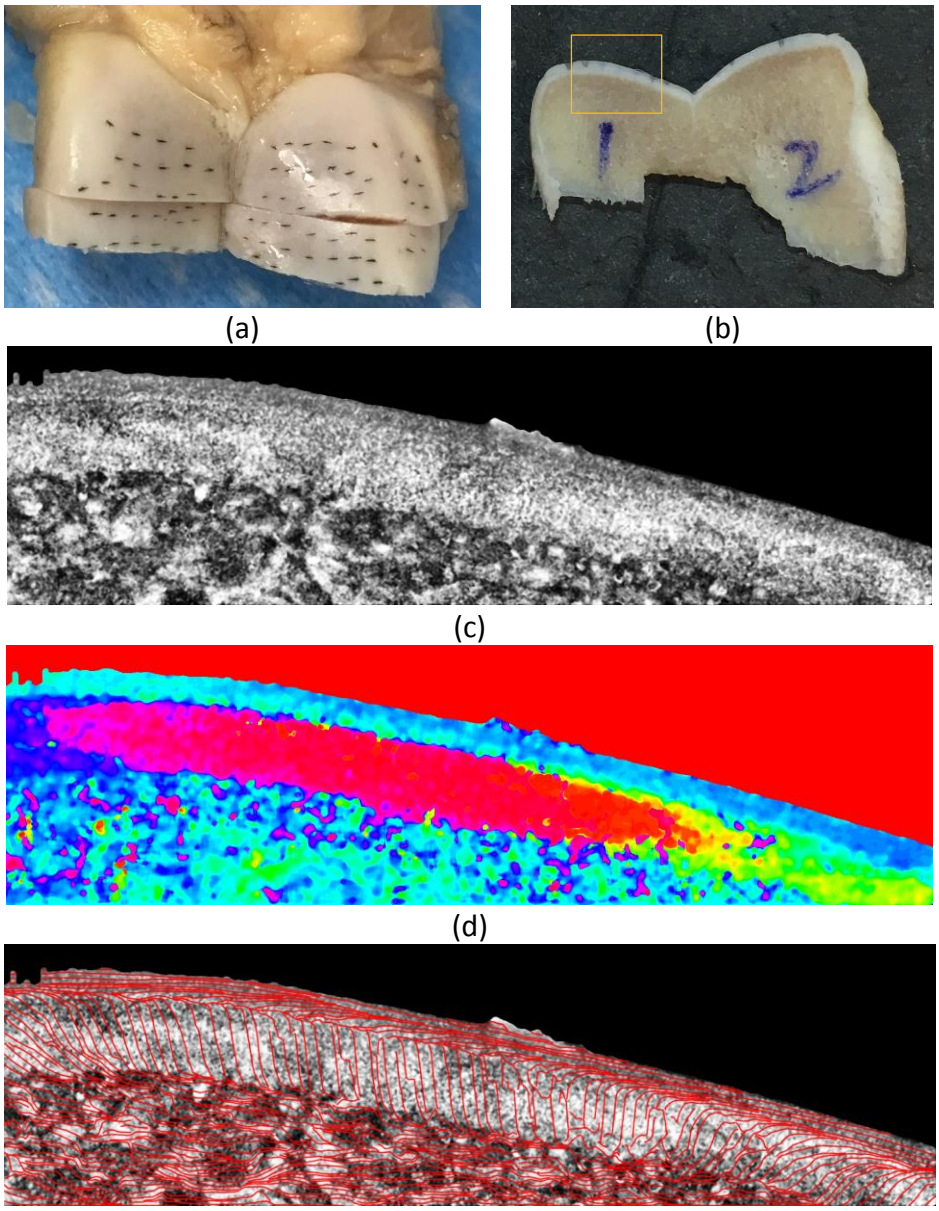

Figure 3-9. (a) Decalcified sample was cut from the sample shown in Figure 3-2; (b) Mark 1 part was the sample #0105161. The images obtained from the yellow squared area are shown with (c) intensity image, (d) optical axis, and (e) streamline plotted on intensity image at transmural depth of 180μm.

The results from side scanning are shown with intensity image, streamline and the optical axis image at transmural depth 180μm above (Figure 3-9 (c-e)) and other depth shows the similar result, all the images are oriented to match with the original sample image. The cartilage part can be easily identified in the intensity image. In the

optical axis image, there is a clear blue layer from the top representing the fiber orientation close to 0 degree, then it turns into purple in the left part and yellow in the right part which represents the absolute value of angle is close to 90˚. The thickness of cartilage measured from the intensity image is ranging from 490μm to 560μm. As an estimation of the superficial layer thickness, the blue layer in the optical axis image had a thickness ranging from 90μm to 120μm.

3.7.2. Histology Validation

Histology results were obtained from sample # 01051601. After over 24 hours' decalcification, the cartilage sample was embedded in wax. Then it was cut at the 200μm from the beginning surface with 40 cuts and each cut created a section with a 5μm thickness and stained using hematoxylin and eosin (H&E). Microscopic images were acquired using a Nikon Eclipse E800 microscope equipped with a color QImaging RETIGA 1300 camera with 10x and 20x magnification, the result was shown as below.

The resolution of 10x lens is 1.0μm per pixel. From the image of histology slide above it's easy to distinguish the cartilage part from the bone. And the thickness of cartilage measured from histology image is ranging from 500μm to 560μm.

For clearer representing the superficial layer, the histology slide was also viewed by a 20x lens with resolution 0.5μm per pixel. At a higher resolution it is able to distinguish the superficial layer with flatted ellipsoid chondrocyte cells. And the thickness of superficial layer measured from histology image is ranging from 95μm to 115μm. The results of thickness measured from histology image are almost the same

with the thickness measured from intensity image and axis image. This suggests that OPT is able to provide a reliable reference about thickness of cartilage and thickness of superficial layer.

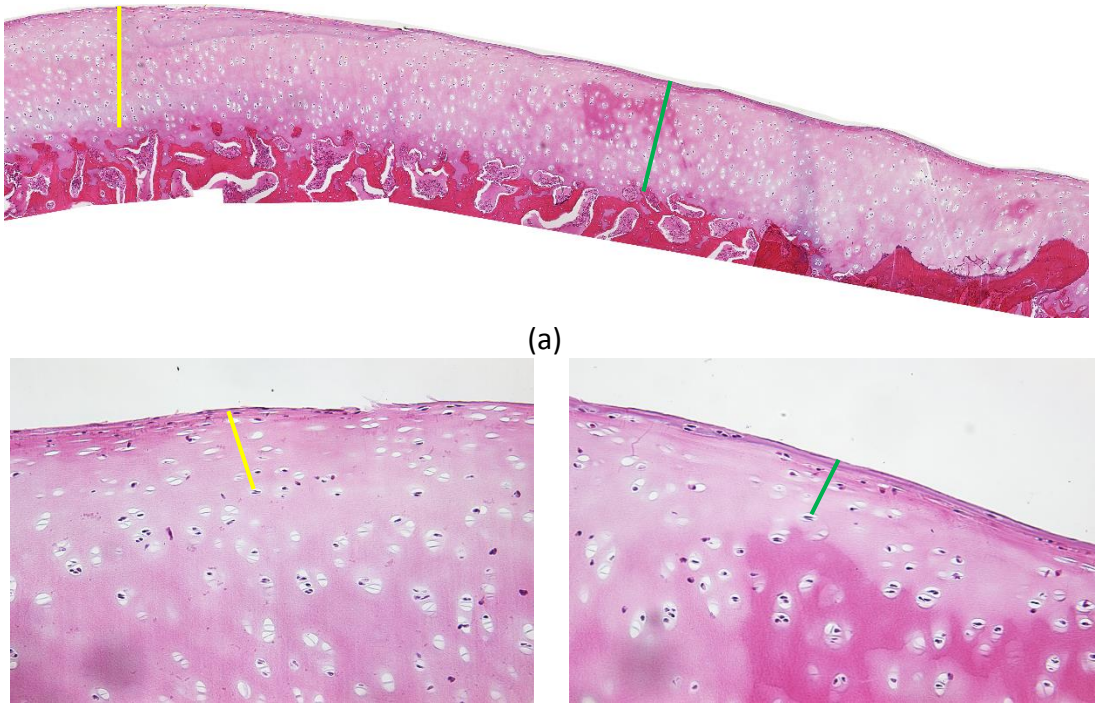

(a)

(b) (c)

Figure 3-10. (a) Cartilage histology image with H&E stain shown in 10x magnification. Yellow line marks the thickness of 560µm, green line marks the thickness of 500µm; (b) Cartilage histology image was shown in 20x magnification. Yellow line marks the superficial layer and thickness here is 115µm; (c) Cartilage histology image was shown in 20x magnification. Green line marks the superficial layer and thickness here is 95µm.

3.7.3. Thickness Measurement Summary

From OPT top scan, it is able to measure the thickness of cartilage and superficial zone from local retardation profile. And the result was validated by histology image and the OPT side scan.

Table 3-1. Summary of Cartilage Thickness Measurement

Methods	Thickness of cartilage (μm)	Thickness of Superficial Zone (μm)
OPT Top scan Local Retardation(1-D)	~580	~120
Histology	500 ~ 560	95 ~ 115
OPT Side scan	490 ~ 560	90 ~ 120

From the Table 3-1, it is clear that with a slight difference the result of thickness measurement is consistent among three different methods, which verified that OPT can obtain the thickness parameter of cartilage as a non-destructive method.

3.7.4. The goodness of fitting

In order to confirm whether the fitting method is reliable, there are two parameters, R-squared (coefficient of determination), Root mean squared error (standard error) used to evaluate the goodness of fitting. The histogram of R^2 and RMSE of sample # 01051601 with 28 data points are shown in Figure 3-11.

Since the fitting method we used here will show better reliability when the angle of split line is larger than 20 degree or smaller than -20 degree, while the majority axis of the sample # 01051601 falls between -10° to 5°. It suggests that the value of R^2 may not be a good indicator of the fitting goodness. So we combine the results of RMSE with R^2 to evaluate the fitting result. From the histogram of R^2, there are 82% (23/28) data points have a value greater than 0.5 which indicates a reliable fit. From the histogram of RMSE, it shows a stable result that all the RMSE values are less than 3, and 75% (22/28) data points have a value equal or lower than 2, which suggests that the error is pretty

small.

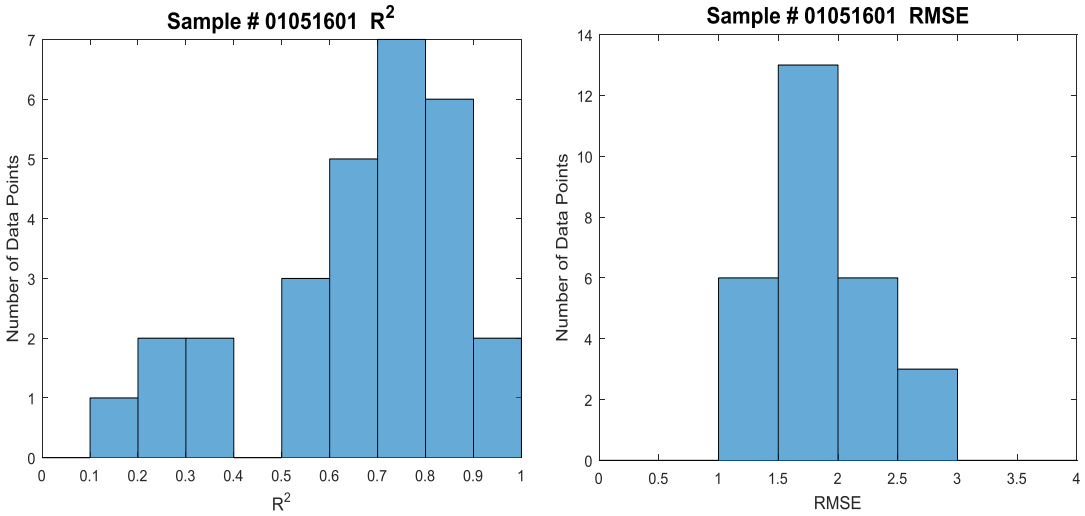

(a) (b)

Figure 3-11. (a) Histogram of R^2 from sample #01051601; (b) Histogram of RMSE from sample #01051601.

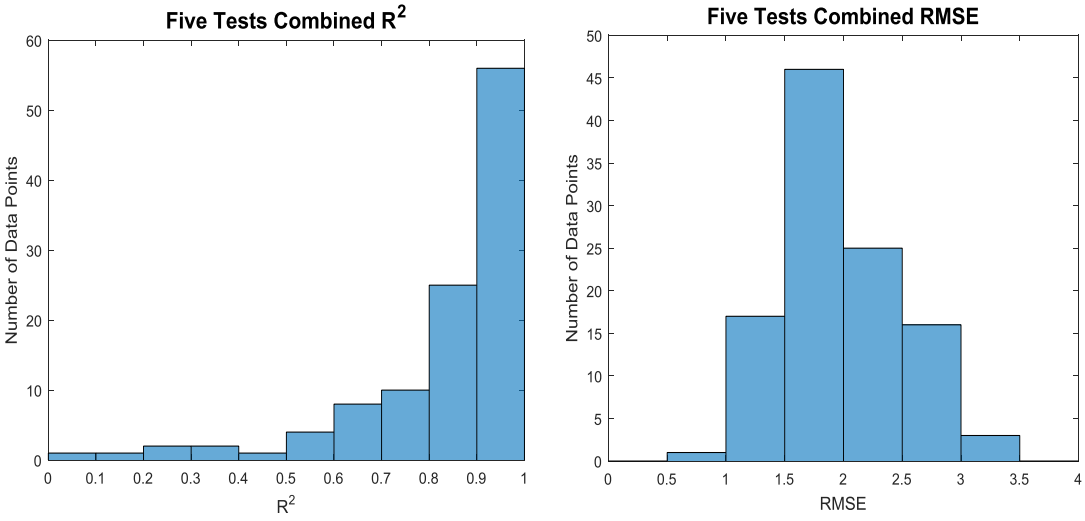

(a) (b)

Figure 3-12. (a) Histogram of combined R^2 from all five samples; (b) Histogram of combined RMSE from all five samples.

The histogram of RMSE and histogram of R^2 of all 112 data points (Figure 3-12) indicate that majority of the data points have the reliable fitting results. There are 7

points (7/112) whose R^2 value is lower than 0.5, and only one point whose RMSE value is higher than 5.

3.8. Summary

The current study aimed to investigate whether OPT is able to replace the split line method and visualize the fiber orientation in articular cartilage superficial zone and the thickness of superficial layer. Both parameters play important roles in regulating the mechanical properties of the articular cartilage and are important factors for better osteochondral plug transplantation. [46,47] An imaging tool that can reveal the microstructures is valuable for a better understanding of the structural-functional relationship in cartilages.

Split line method can visualize the predominant collagen fiber orientation in the cartilage top layer; however, it has several limitations. First of all, split line is a destructive method that damages the sample. Second, the quality of split line pattern is strongly related with the choice of needle. If the needle has a relatively thick tip, the pattern of split line will show curved, sharply angled, forked or stellate shape of patterns as mentioned in introduction chapter, which can't be distinguished as a trend of fiber. Even the needle is appropriate enough, a delicate operation is required that poking the sample at exact 90° to the joint surface, it becomes more difficult when the sample is relative small. Last and the most important, the pattern of split line is static. Previous study shows that articular cartilage is able to response to the loaded stress, there is reorganization of collagen mesh works within the response, which is the

characterization that split line cannot tell.

OPT, as an imaging modality developed from Jones matrix PS-OCT, is able to provide non-destructive image result in real time, which means it can visualize the alterations in articular cartilage during different loading tests without damaging the sample.

Compared to the conventional PS-OCT, OPT in this study is better in two ways. First, OPT offers the "local" optical axis instead of "cumulative" optical axis from conventional PS-OCT. Second, OPT cooperated the advanced rendering method to visualize the optical axis as fiber orientation which is valuable in helping understanding the complicated microstructure in articular cartilage.

In correlation analysis between angle of split line and the optical axis from sample #01051601, the R^2 shows a depth-varying value and achieves the relatively high value from 48μm to 120μm. Similar results were obtained in other samples.

In order to figure out the reason that the poor correlation between 0-48 μm, the *en face* cumulative retardation images were checked and shown as below (Figure 3-13(a,c,e)). From 4μm to 48μm, the local retardation increased which indicates the birefringence alteration within these depths. From the streamline images (Figure 3-13 (b,d,f)), it is clear that fiber orientation changes during depth 4μm to 48μm which explains why the correlation is low in this interval.

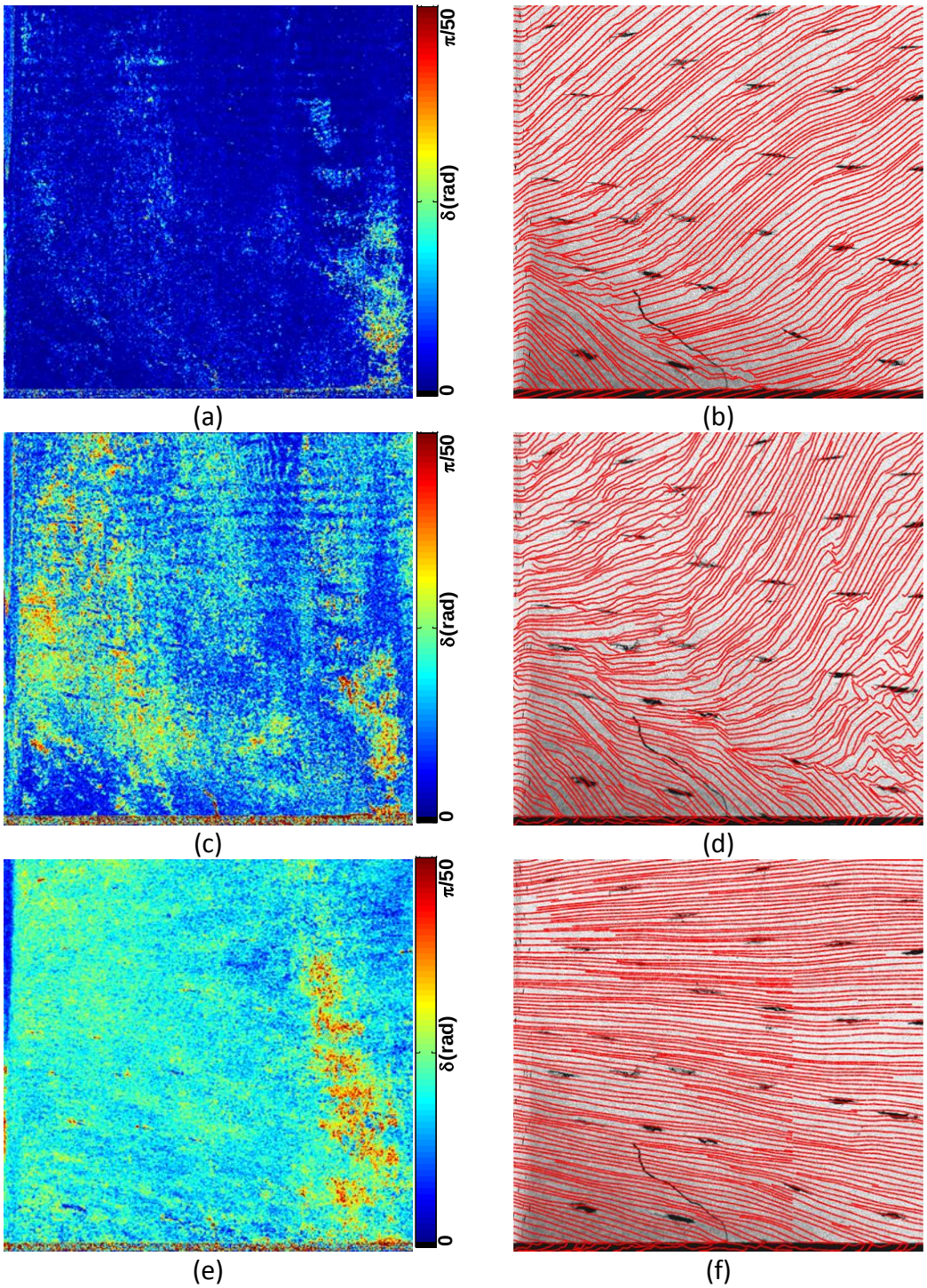

Figure 3-13. *en face* local retardation and tractographic images of Sample #01051601 obtained at (a, b) 4µm depth; (c, d) 20µm depth; and (e, f) 48µm depth.

In the deeper zone after superficial layer it is known that fiber orientation change from parallel to surface into perpendicular to the surface, which explains the low

correlation after 120μm.

In addition to fiber orientation, OPT also measures the cartilage thickness and the thickness of the superficial layer, which are important in clinical evaluation. In order to optimize the longevity of grafts in autologous osteochondral transplantation, selection of transplants with the same cartilage thickness as the host bed might prevent early graft degeneration. [7] As previous study verified that thickness is inhomogeneous among the different sites in articular cartilage. [13]

Based on the clear difference between cartilage and bone, the thickness of cartilage is relatively easy to measure from the intensity image, and the result obtained from side scan on sample #01051601 is in the range of 490μm to 560μm with the resolution of 4μm per pixel, meanwhile the result measured from histology image is 500μm to 560μm with the resolution of 0.5μm per pixel with a 20x magnification lens. With only 2% error, OPT provides a histology-accurate thickness measurement.

However, because the histology image can't separate the superficial zone with other zones using H&E stain, the thickness of superficial zone is measured based on the shape of chondrocyte cells roughly. Measuring from the surface to the flatted ellipsoid chondrocyte cells layer, the result is ranging from 95μm to 115μm.

From the optical axis result of sample side scanning, it is clear to see a layer fiber with orientation parallel to the surface. In sample #0105161, this thickness was measured as 90μm to 120μm from the "side" scan. This result is consistent with the result obtained in the correlation analysis where the R^2 started to drop from 0.71 to 0.57 at 120μm, indicating a big alteration in fiber orientation.

Chapter 4. Conclusions and Future Studies

We showed in this study that OPT provides a non-destructive alternative to the destructive “split line” method for visualizing the fiber orientation in the top layer of articular cartilage. Without damaging the sample and avoiding the delicate procedures for preparing the split line pattern, OPT can provide a more stable optical axis result which representing the fiber trend in real time.

In addition, as an OCT based imaging method, OPT can also measure the cartilage thickness from different sites of the scanning area with a histology-level accuracy. Furthermore, OPT can reveal the thickness of the superficial cartilage based on local retardance values. These parameters are valuable in clinical therapy such as in osteochondral transplantation surgery.

There are still some unanswered questions in the correlation analysis. The correlation is low from the cartilage surface to the depth of 32μm. However, the side imaging result indicated a relatively homogeneous superficial layer parallel to the surface within the same depth range. It is possible that the first several layers have different angles in 3D. Therefore further studies are needed to fully understand the 3D microstructure in articular cartilage. Nevertheless, OPT has shown great potential for evaluate cartilage properties that are valuable for both basic research and clinical applications.

References

1 Temenoff, J.S. and A.G. Mikos, Review: tissue engineering for regeneration of articular cartilage. Biomaterials, 2000. 21(5): p. 431-440.

2 Buckwalter, J.A., H.J. Mankin, and A.J. Grodzinsky, Articular cartilage and osteoarthritis. Instructional Course Lectures-American Academy of Orthopaedic Surgeons, 2005. 54: p. 465.

3 Bhosale, A.M. and J.B. Richardson, Articular cartilage: Structure, injuries and review of management. British Medical Bulletin, 2008. 87(1): p. 77-95.

4 Poole, C. A. (1997). Review. Articular cartilage chondrons: form, function and failure. Journal of anatomy, 191(1), 1-13.

5 Nesic, D., et al., Cartilage tissue engineering for degenerative joint disease. Advanced Drug Delivery Reviews, 2006. 58(2): p. 300-322.

6 Chu, C. R., Williams, A., Tolliver, D., Kwoh, C. K., Bruno, S., & Irrgang, J. J. (2010). Clinical optical coherence tomography of early articular cartilage degeneration in patients with degenerative meniscal tears. Arthritis & Rheumatism, 62(5), 1412-1420.

7 Zeissler, M., et al., Cartilage thickness and split-line pattern at the canine humeral trochlea. Veterinary and Comparative Orthopaedics and Traumatology, 2010. 23(5): p. 343-347.

8 Özmeriç, A., Alemdaroğlu, K. B., & Aydoğan, N. H. (2014). Treatment for cartilage injuries of the knee with a new treatment algorithm. World Journal of Orthopedics, 5(5), 677–684. http://doi.org/10.5312/wjo.v5.i5.677

9 Bobić, V. (1996). Arthroscopic osteochondral autograft transplantation in anterior cruciate ligament reconstruction: a preliminary clinical study. Knee Surgery, Sports Traumatology, Arthroscopy, 3(4), 262-264.

10 Kock, N. B., Van Susante, J. L., Buma, P., Van Kampen, A., & Verdonschot, N. (2006). Press-fit stability of an osteochondral autograft: influence of different plug length and perfect depth alignment. Acta orthopaedica, 77(3), 422-428.

11 Braun, Hillary J., and Garry E. Gold. "Diagnosis of osteoarthritis: imaging." Bone 51.2 (2012): 278-288.

12 Eckstein, F. et al. “Imaging of Cartilage and Bone: Promises and Pitfalls in Clinical Trials of Osteoarthritis.” Osteoarthritis and cartilage / OARS, Osteoarthritis

Research Society 22.10 (2014): 1516–1532. PMC. Web. 7 Apr. 2016.

13 Boettcher, Peter, et al. "Mapping of Split‐Line Pattern and Cartilage Thickness of Selected Donor and Recipient Sites for Autologous Osteochondral Transplantation in the Canine Stifle Joint." Veterinary Surgery 38.6 (2009): 696-704.

14 Bae, Won C., et al. "Wear-lines and split-lines of human patellar cartilage: relation to tensile biomechanical properties." Osteoarthritis and Cartilage 16.7 (2008): 841-845.

15 Meachim, G., et al., Collagen alignments and artificial splits at the surface of human articular cartilage. Journal of anatomy, 1974. 118(Pt 1): p. 101.

16 Petersen, W. and B. Tillmann, Collagenous fibril texture of the human knee joint menisci. Anatomy and embryology, 1998. 197(4): p. 317-324.

17 Cowin, Stephen C., and Stephen B. Doty. "Chapter 14." Tissue Mechanics. New York: Springer, 2011. 484-85. Web.

18 Below, S., et al., The split-line pattern of the distal femur: a consideration in the orientation of autologous cartilage grafts. Arthroscopy: The Journal of Arthroscopic & Related Surgery, 2002. 18(6): p. 613-617.

19 Mononen, M.E., et al., Effect of superficial collagen patterns and fibrillation of femoral articular cartilage on knee joint mechanics-A 3D finite element analysis. Journal of Biomechanics, 2012. 45(3): p. 579-587.

20 Li, LePing, J. T. M. Cheung, and W. Herzog. "Three-dimensional fibril-reinforced finite element model of articular cartilage." Medical & biological engineering & computing 47.6 (2009): 607-615.

21 Brill, Nicolai, et al. "3D Human cartilage surface characterization by optical coherence tomography." Physics in medicine and biology 60.19 (2015): 7747.

22 Fercher, Adolf F., et al. "Optical coherence tomography-principles and applications." Reports on progress in physics 66.2 (2003): 239.

23 Beard, Paul. “Biomedical Photoacoustic Imaging.” Interface Focus 1.4 (2011): 602–631. PMC. Web. 7 Apr. 2016.

24 Xie, Tuqiang, et al. "Use of polarization-sensitive optical coherence tomography to determine the directional polarization sensitivity of articular cartilage and meniscus." Journal of biomedical optics 11.6 (2006): 064001-064001.

25 Jones, R. Clark. "A New Calculus for the Treatment of Optical SystemsI. Description and Discussion of the Calculus." JOSA 31.7 (1941): 488-493.

26 Pircher, Michael, Christoph K. Hitzenberger, and Ursula Schmidt-Erfurth. “Polarization Sensitive Optical Coherence Tomography in the Human Eye.” Progress in Retinal and Eye Research 30.6 (2011): 431–451. PMC. Web. 7 Apr. 2016.

27 Gramatikov, Boris I. "Modern technologies for retinal scanning and imaging: an introduction for the biomedical engineer." Biomedical engineering online 13.1 (2014): 52.

28 Chu, Constance R., et al. "Arthroscopic microscopy of articular cartilage using optical coherence tomography." The American journal of sports medicine 32.3 (2004): 699-709.

29 Saarakkala, Simo, et al. "Quantification of the optical surface reflection and surface roughness of articular cartilage using optical coherence tomography." Physics in medicine and biology 54.22 (2009): 6837.

30 Nebelung, Sven, et al. "Three‐dimensional imaging and analysis of human cartilage degeneration using Optical Coherence Tomography." Journal of Orthopaedic Research 33.5 (2015): 651-659.

31 Nebelung, Sven, et al. "Morphometric grading of osteoarthritis by optical coherence tomography—an ex vivo study." Journal of Orthopaedic Research 32.10 (2014): 1381-1388.

32 Ugryumova, Nadya, et al. "The collagen structure of equine articular cartilage, characterized using polarization-sensitive optical coherence tomography." Journal of Physics D: Applied Physics 38.15 (2005): 2612.

33 Li, Xingde, et al. "High-resolution optical coherence tomographic imaging of osteoarthritic cartilage during open knee surgery." Arthritis research & therapy 7.2 (2005): R318.

34 Chu, Constance R., et al. "Clinical diagnosis of potentially treatable early articular cartilage degeneration using optical coherence tomography." Journal of biomedical optics 12.5 (2007): 051703-051703.

35 Lu, Zenghai, Deepa Kasaragod, and Stephen J. Matcher. "Conical scan polarization-sensitive optical coherence tomography." Biomedical optics express 5.3 (2014): 752-762.

36 Matcher, Stephen J. "What can biophotonics tell us about the 3D microstructure of articular cartilage?" Quantitative imaging in medicine and surgery 5.1 (2015): 143.

37 Wang, Yuanbo, and Gang Yao. “Optical Tractography of the Mouse Heart Using Polarization-Sensitive Optical Coherence Tomography.” Biomedical Optics Express 4.11 (2013): 2540–2545. PMC. Web. 14 Apr. 2016.

38 Azinfar, Leila, et al. "High resolution imaging of the fibrous microstructure in bovine common carotid artery using optical polarization tractography." Journal of biophotonics (2015).

39 Fan, Chuanmao, and Gang Yao. "Single camera spectral domain polarization-sensitive optical coherence tomography using offset B-scan modulation." Optics express 18.7 (2010): 7281-7287.

40 Fan, Chuanmao, and Gang Yao. "Full-range spectral domain Jones matrix optical coherence tomography using a single spectral camera." Optics express 20.20 (2012): 22360-22371.

41 Fan, Chuanmao, and Gang Yao. "Imaging myocardial fiber orientation using polarization sensitive optical coherence tomography." Biomedical optics express 4.3 (2013): 460-465.

42 Arokoski, J. P., et al. "Decreased birefringence of the superficial zone collagen network in the canine knee (stifle) articular cartilage after long distance running training, detected by quantitative polarised light microscopy." Annals of the rheumatic diseases 55.4 (1996): 253-264.

43 Kiraly, K., et al. "Specimen preparation and quantification of collagen birefringence in unstained sections of articular cartilage using image analysis and polarizing light microscopy." The Histochemical journal 29.4 (1997): 317-327.

44 Xia, Y., et al. "Quantitative in situ correlation between microscopic MRI and polarized light microscopy studies of articular cartilage." Osteoarthritis and Cartilage 9.5 (2001): 393-406.

45 Wilson, Wouter, et al. "The importance of the collagen network architecture in articular cartilage for the mechanical loading of individual collagen fibrils." 2003 ASME summer bioengineering conference/Ed. LJ Soslowsky, TC Skalak, JS Wayne, GA Livesay. ASME, 2003.

46 Moutos, Franklin T., Lisa E. Freed, and Farshid Guilak. "A biomimetic three-dimensional woven composite scaffold for functional tissue engineering of cartilage." Nature materials 6.2 (2007): 162-167.

47 Knecht, Sven, Benedicte Vanwanseele, and Edgar Stüssi. "A review on the mechanical quality of articular cartilage–Implications for the diagnosis of osteoarthritis." Clinical biomechanics 21.10 (2006): 999-1012.

Appendix

```
function Creat_Mask()
%% Mask Generation Function
%  Author: Xuan Yao
%  xy364@mail.missouri.edu
%  University of Missouri

%% Load the file
dir='D:\Xuan_Yao\Cartilage\1-5-2016\test1\3D\';
filenameI='IT3D_interp.dcm';
filenameA='LTAxis_3D_interp.dcm';

volI=dicomread([dir,filenameI]);
volA=dicomread([dir,filenameA]);

n=input(' Number of Split Lines: ');


idx=20;

%% Mean imgI
volI=squeeze(volI);
tempVolI=volI(12:60,:,:); % Average intensity from 48micron to
240micron
tempVolI=double(tempVolI);
imgI=squeeze(mean(tempVolI,1));
imgI=mat2gray(imgI,[0,255]);
imgI=imadjust(imgI,[0.3 0.6]); % Increase the contrast of the imgI
figure(2),imagesc(imgI);colormap(gray);axis off % Show the intensity

%% Create the binary ROI of split line base on intensity
for i=1:n
    Bw{i}=roipoly(imgI);
    hold on
end

%% Generate the mask from greyscale image
for i=1:n
    I_new{i} = imgI.*Bw{i};% Get the greyscale image of ROI
    I_new{i}(Bw{i}==0)=1;
    BW_new{i} = (I_new{i} < 0.7);% Obtain the split line by Intensity
    BW_new1{i}=medfilt2(double(BW_new{i}),[7,7]);
   figure,imshow(BW_new1{i}); axis off % Check the mask

end

%% Save the mask in .mat format
save ('Mask_1-5-1.mat','BW_new1','-v6');
```